Doctoral Dissertation (Shinshu University)

Study on structure and mechanical properties of spider dragline silk fibers

September 2013

Lei Zhang

CONTENTS

Chapter 1

General Introduction

Chapter 1: General Introduction

Bio-macromolecular fibers were used in textile, medicine and biology because of their intrinsic bio-function. And for many years the polymer industry had attempted to produce synthetic textile fibers that match the many desirable properties of the cocoon silks made by the silk moths, *Bombyx mori* and *Antheraea pernvi.* Many of the synthetic, like nylon, are chemically similar to silk, and in many respects their properties approach or exceed those of silk. But because of the unique combination of high strength, superb texture, and the ability to bind a wide variety of chemical dyes, silk remains the premier textile material of the fashion industry. As a consequence, the mass culture of silk moths remains a major industry in many countries (Gosline et al. 1986).

Spider silks have been known for long to possess extraordinary mechanical properties. Spiders have been using protein-based nanomaterials with the ability to self-assemble into fibers and sheets for over 450 million year (Lewis, 2006). Spiders are unique because of the use of silks throughout their life span and their nearly total dependence on silk for their evolutionary success (Lucasd, 1964; Vollrath, 1992). Because of the extreme properties of spider silk, with tensile strength roughly equivalent to that of high-grade steel, it is also highly ductile, capable of stretching up to 4 times its normal length without breaking, it maintains these properties over a wide range of temperatures and is only about 1/5 as dense as steel. Moreover, spider

silks fibers are biocompatible and biodegradable. Thus, spider silk fibers have been applied in various field such as military (bullet-proof vests), aviation (parachute cords), medical science (surgical sutures, replacement ligaments) etc. Recently, with the development of biological technology, the artificial protein of spider silk was successfully with gene transplanting and the artificial spider silk was spun. The developments of these technologies accelerate the pace of application of spider silk.

Spiders also have evolved the ability to produce the ability to produce as many as six different silk fibers that have differing tensile strengths and elasticities. The typical orb-shaped spider web is constructed from different silks, each of which is produced in a separate gland: the major and minor ampullate glands (locomotion and web frame), tubuliform (egg case silk), flagelliform (spiral capture silk), aciniform (prey wrapping silk), aggregate (sticky adhesives on spiral capture or gumfooted lines), and the pyriform glands (attachment disc and joining fibers). Fig. 1-1 (Vollrath 1992, 2000) gives an overview of the different types of spider silks and their function for the orb-web weaving spider *Araneus diadematus.* And Fig. 1-2 gives a microdissection of the silk-producing glands from the abdomen of *Nephia. clavipes*. Among these silks, the most investigated type of spider silk is the dragline or major ampullate (MA) silk that is secreted by the major ampullate glands of the spider. The dragline is used to support the spider when constructing a web and to prevent it from falling. This function results in mechanical properties combining a high Young's modulus with a high strength.

Although each of the silk glands has its own distinctive shape and size, they are

functionally organized in a similar pattern (Fig.1-3) (Römer and Scheibel, 2008). The majority of the gland is a reservoir of soluble silk protein synthesized in specialized cells at the distal end of the gland and secreted into the lumen of the gland. The soluble silk is then pulled down a narrow duct during which physical and chemical changes occur, producing the solid silk fiber. A muscular valve is present at the exit to the spinneret that can control the fiber diameter. The silk exits through spigots on the spinnerets, of which there are three pair: anterior, median, and posterior, each specific for a silk type (Lewis, 2006; Lucas, 1964; Foelix, 1996).

Silks are macromolecular composites of amorphous protein domains that are cross-linked and reinforced by β-sheet microcrystals; the degree of crystalline cross-linking and reinforcement largely determines functionally important mechanical properties. Factors that influence the formation and size of the crystal include the primary and secondary structure of the proteins, control of the genes that encode these proteins, and the chemical and mechanical processing of the proteins during spinning (Guerette et al., 1996).

The proteins that comprise the silks and their sequences have provided key information that relates directly to those extraordinary properties. Spider silks are composed of proteins that generally show a repetitive core region flanked by non-repetitive N- and C- terminal domains (Hayashi and Lewis, 2001; Motriuk-Smith et al., 2005). Spider silks are composed of its amino-acid composition, a majority of the residues have short or no side chain (Ala, Gly) (Casem et al., 1999; Peakall, 1969). When detailed studies of spider silk protein were started, the amino acid compositions

for a number of spider silks and mechanical test data were the only information available.

The first cDNA sequence for a spider silk protein from the major ampullate silk of *Nephila clavipes,* termed MaSp1 (Fig. 1-4), was published in 1990 (Xu and Lewis). That partial sequence contained similar but nonidentical repeats with sequence motifs including stretches of polyAla of up to seven residues alternating with $(GGX)_n$ sequences (G, glycine; A, alanine; Xu and Lewis, 1990), where the X residues are Y, L, and Q in that sequence order. There are differences in the number of GGX units in each repeat, but there are virtually no substitutions for the three X amino acids.

The second major ampullate silk protein was found on the basis of the identification of a proline-containing peptide in the silk, which was absent from protein encoded by the cDNA for MaSp1. This led to the cDNA for the second major ampullate silk protein, MaSp2 (Hinman and Lewis, 1992) (Fig. 1-4). The repetitive sequence and predicted structure of this protein forced a rethinking of the mechanism for elasticity and tensile strength. The novel sequence features in the consensus repeats of this protein include the polyAla regions as in MaSp1 alternating with sequences of GPGQQGPGGY (P, proline; Q, glutamine; Hayashi et al., 1999). As with MaSp1, virtually no amino acid substitutions occur in the repetitive region. The repeats are the consensus of the hundreds of repeats in the protein, and most repeats have minor differences from the consensus either in the number of three or five amino acid motifs or the number of alanine residues in the polyAla motif.

Among these motifs in MaSp1 and MaSp2, and polyAla are major components of

the β-sheet crystal structure (Gosline et al., 1999), and they are regarded as being responsible for the tensile strength of the silk (Winkler and Kaplan, 2000) as the large number of hydrogen bonds, combined with the hydrophobic forces due to the absence of water in these regions, provides a large force preventing the silk molecules from separating (Parkhe et al., 1997). Computer models of the polyAla segment shown in Fig. 1-5 (Lewis, 2006). The GGX repeat regions might form helix structures that function as linkages between crystalline and non-crystalline portions of the molecule, or function to help align protein molecules in the silk (Hayashi et al., 1999; Kummerlen et al. 1996; Dong et al. 1991). Computer model of the GGX repeat region show in Fig. 1-6 (Lewis, 2006). The MaSp2 protein exhibits GPGXX and GPGQQ motifs formed β-turn spirals of the dragline silk (Hayashi et al., 1999) and, thus are responsible for the extensibility of the silk. Studies have suggested that MaSp1 is more prevalent in the spider dragline silk than MaSp2, with a ratio of approximately 3:2 or higher, depending on the species (Brooks et al., 2005, Hinman et al., 1992, Sponner et al., 2005). Thus, the mechanical properties of spider silks are thought to be conferred largely to the secondary structure of amino acid motifs in the repetitive part of proteins.

The structure of spider silk was first proposed to consist of antiparallel sheets by Pauling and Corey (1953).Although this has been shown to be correct there exist various other conformations and folding patterns, and a full structural elucidation is still being sought 40 years later. Termonia (1994) proposed that spider silk is a semicrystalline material made of amorphous flexible chains reinforced by tiny,

virtually undeformable, crystals. Molecular studies of dragline silk (Bram et al., 1997, Gillespie; Viney and Yager, 1994; Simmons, Ray and Jelinski, 1994; Dong, Lewis and Middaugh, 1991, Lawrence, Vierra and Moore, 2004) have shown that spider dragline silk structural model at the moment is that the poly-alanine regions form β-sheet which stack to form crystals in an amorphous glycine-rich matrix. Simmons et al. (1996) concluded from NMR spectra that the two crystalline fractions were found to be either highly oriented or poorly oriented and less densely packed. On population, representing about 40% of the alanine residues, is composed of highly orientted alanine-rich crystals. The other population (60%) consists of poorly oriented and less densely packed 'protocrystal', probably preformed β-sheet. In addition, the model for the molecular structure of spider dragline silk was established where two crystalline fractions composed of stretches of alanine were embedded in a glycine rich amorphous matrix. The model shows in Fig. 1-7.

The unusual mechanical properties are the key features attracting researchers to spider's silks. Spiders appear to use the minimum amount of silk necessary in their webs to catch prey. The web has to stop a rapidly flying insect nearly instantly, so that the prey becomes entangled and trapped. To do this, the web must absorb the energy of the insect without breaking and yet not act as a trampoline and bounce the insect away from the web. Gosline et al. reviewed several aspects of this property and concluded that spider silk and the web are nearly optimally designed for each other. Fig.1-8 (Gosline et al. 1999, Vollrath et al.2001) shows typical stress-strain curve of dragline silk. The stress (σ) is the normalized force (F), defined as $\sigma=F/A$, where A is

the initial cross-sectional area of the silk fiber. The strain (ε) is the normalized deformation, defined as $\varepsilon=\Delta L/L_0$, where L_0 is the fiber's initial length, and ΔL is the change in fiber length. The slope of the stress-strain curve gives the stiffness of the material, and the maximum values of stress and strain at the point where the material fails give the strength (σ_{max}) and extensibility (ε_{max}), respectively. The area under the stress-strain curve gives the energy required to quantify toughness. At the point at which permanent deformation starts to take place, called the yield point, the interchain bonds in the amorphous regions can break and the polymer chains begin to slip by each other. Table 1-1 gives a comparison of the mechanical properties of the spider dragline silks with other biological and synthetic materials. In comparison, although the strength and stiffness of dragline silk is lower than the engineering materials, such as Kevlar, carbon and steel fiber, large extensibility of dragline silk makes this silk tougher than these materials.

As with any polymer, especially those composed of protein, there are numerous factors that can affect the tensile strength and elasticity. These can include temperature, hydration state, and extension rate. Due to daily changes in climate lead to spider orb webs are typically rebuilt every day. Another key factor is the diameter of the fiber, which can vary greatly along the length of a single fiber (Cunniff *et al.*, 1994a; Gosline*, et al.*, 1999; Madsen and Vollrath, 2000; Vollrath, Madsen and Shao, 2001). In fact, the mechanical characteristics of spider dragline silk possess variability not only between species, but also with species and even within an individual (Madsen, Shao and Volleth, 1999). In addition, spider silks are highly variable not

only in mechanical properties (Cunniff et al. 1994b, Madsen et al. 1999, Vollrath et al. 2001, Swanson et. al. 2006), but also in chemical composition (Work and Young, 1987, Lombardi and Kaplan, 1990).

In this thesis, I report a variable of the mechanical properties of spider dragline silk at interspecific and intraspecific.

In chapter 2, I describe the mechanical properties of *Argiope amoena* dragline silk obtained by artificial forcible reeling at different speeds. In addition, the conformation and crystalline structure of silk fibers were reported.

In chapter 3, I describe the variable of the mechanical properties of dragline silk fiber from four spider species: *Nephia clavata*, *Nephia pilipes*, *Argiope bruennichi* and *Argiope amoena*. In addition, the molecular structure changes were analyzed using Raman spectra.

In chapter 4, I describe the secondary structure change of *Nephia clavata* dragline silk fiber obtained by different spinning methods.

Table 1-1 Tensile properties of spider dragline silks and other materials

Material	Initial modulus (GPa)	Strength (GPa)	Strain (%)	Toughness (MJ m^{-3})	Ref.
Dragline silk	7-20	0.8-1.8	27-40	96-230	a, b,c
Bombyx mori.silk	7-16	0.5-0.7	12-24	70	d,e
Tendon collagen	1.5	0.15	0.12	7.5	f
Synthetic rubber	0.001	0.05	8.5	100	f
Nylon	5	0.95	0.18	80	f
Kevlar 49	130	3.6	0.027	50	f
Carbon	300	4	0.013	25	f
High-tensile steel	200	1.5	0.008	6	f

Only dragline silks from web building spiders are included.

a,Vollrath et al., 2001a, b, Medsen et al. 1999, c, Sirishaisit, et al. 2003, d, Shao and Vollrath, 2002, e, Tsukada et al. 1996, f, Gosline, et al. 1999.

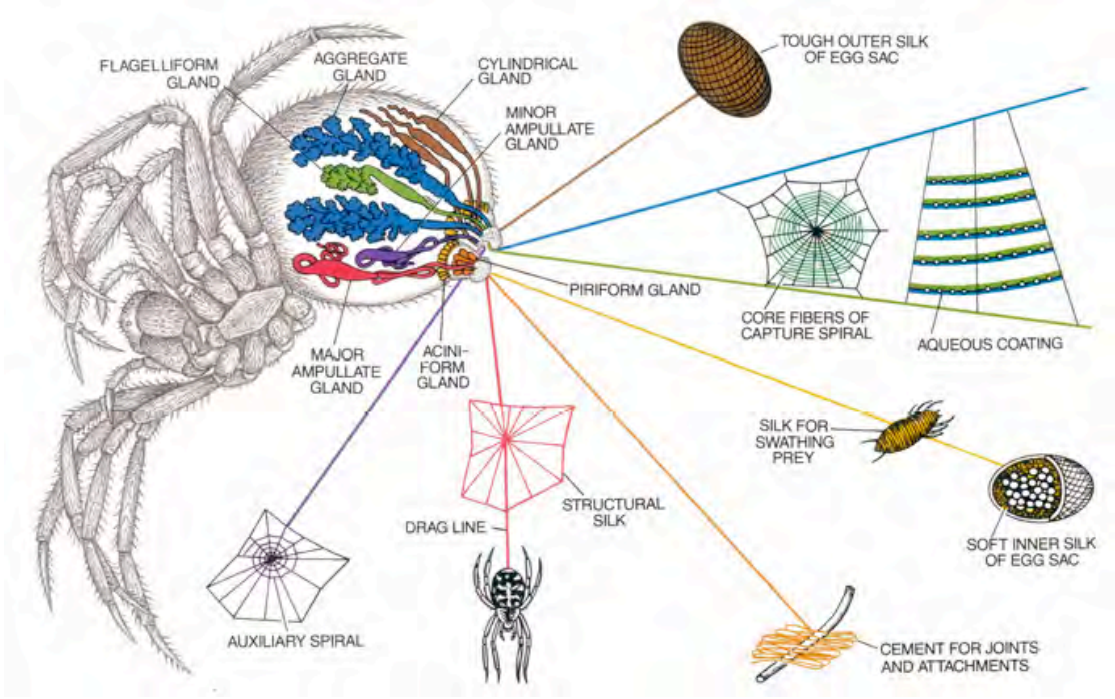

Fig. 1-1. Types and functions of orbweabing spider silk of *Araneus diadematus*. (Vollrath 1992, 2000)

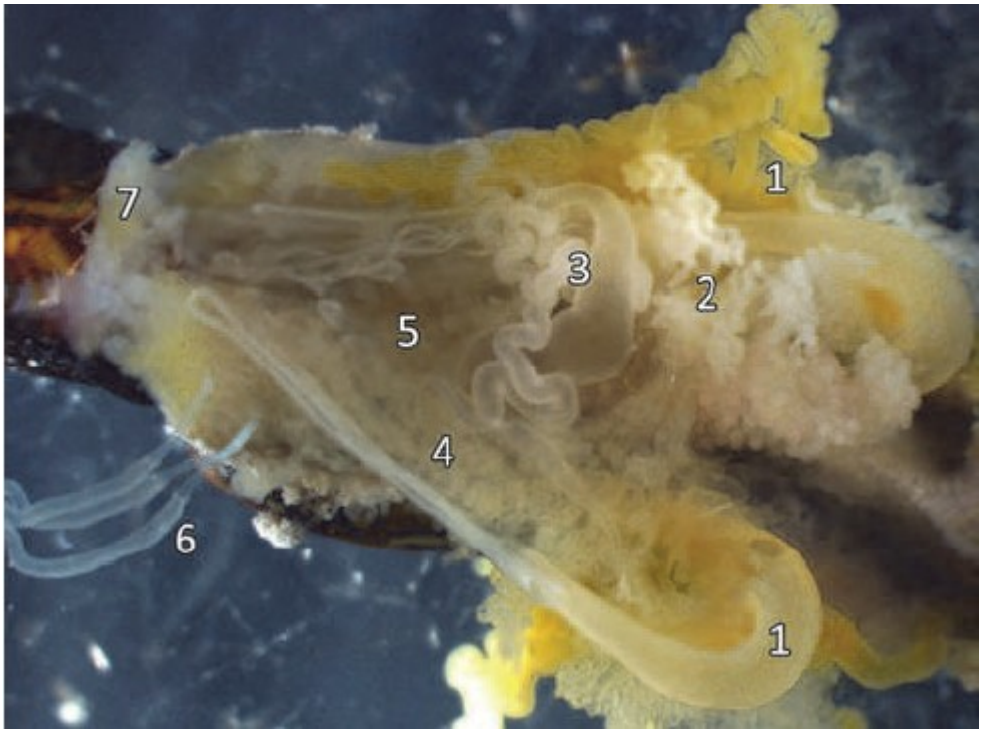

Fig.1-2 Microdissection of the silk-producing glands from the abdomen of *Nephila. clavipes* indicates several specialized structures that manufacture silk fibroins. Numbers indicate each gland: 1 (top and bottom – major ampullate), 2 (flagelliform), 3 (minor ampullate), 4 (aggregate), 5 (aciniform), 6 (tubuliform) and 7 (pyriform).

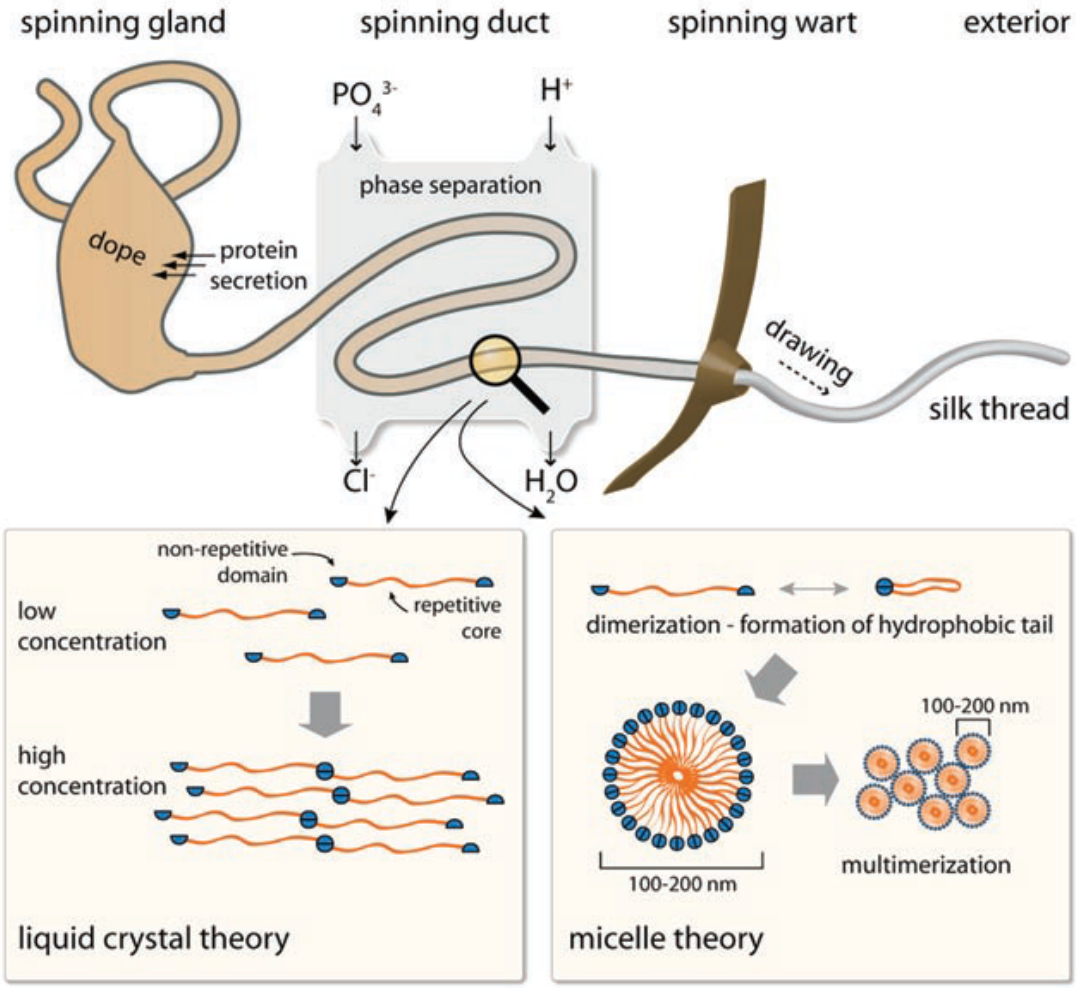

Fig. 1-3 Model of silk spinning process. The highly concentrated spider silk protein solution is secreted and stored inside the spinning gland. Upon initiation of thread formation, the solution is directed through a narrow ion exchange channel, in which a phase separation process takes place. Mechanical drawing of the silk thread (hind legs/gravity) results in rapid assembly of the silk fiber. Two theories exist concerning the molecular process inside the spinning duct. The first theory supports a liquid-crystalline behavior of the silk proteins, whereas the other theory favors a micellar organization of the proteins, before elongation (through laminar force) finally leads to thread assembly. (Römer and Scheibel, 2008)

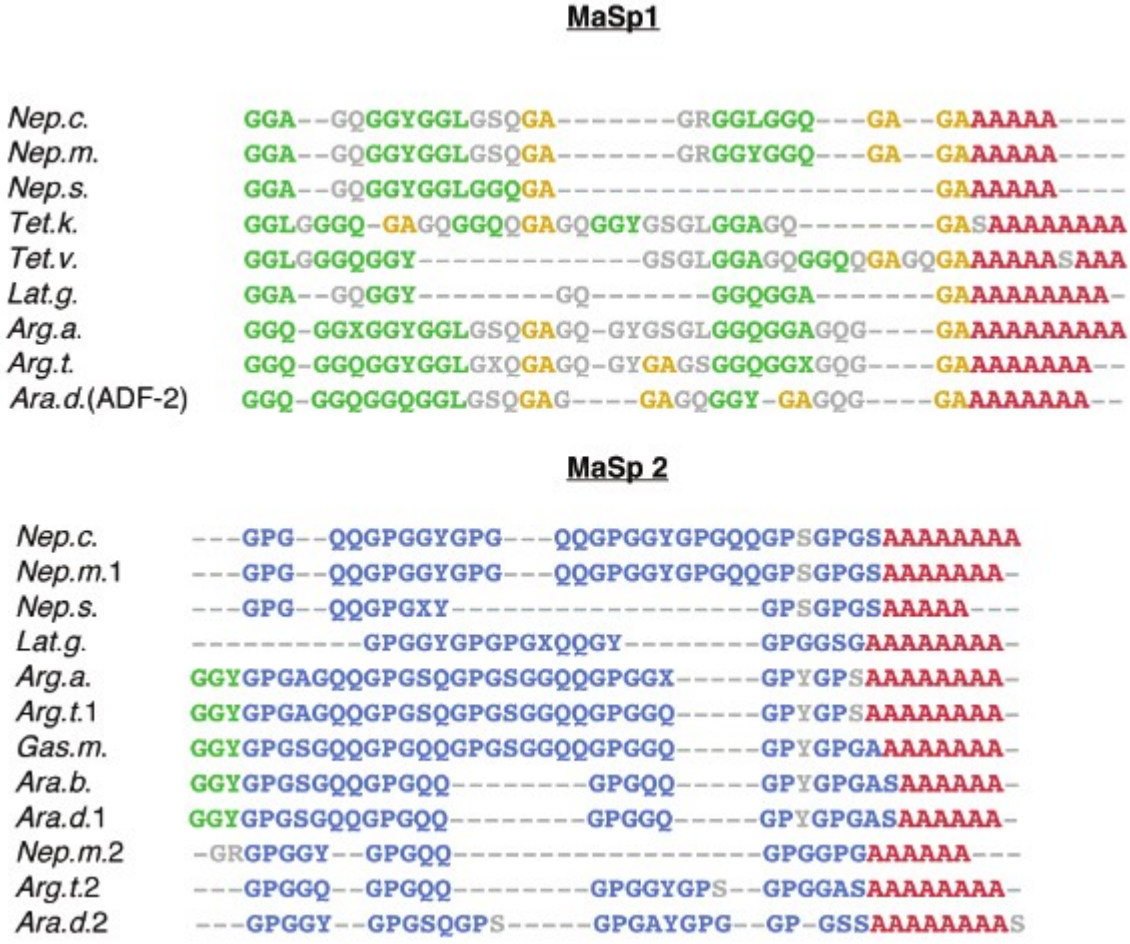

Fig. 1-4 Amino acid sequences of the consensus repetitive sequence of the major ampillate silk proteins in various spider species. Amino acids are denoted in one-letter code. (-) indicates an amino acid not present when compared to the other sequences. Spiders: *Nep. c.*, *Nephila clavipes*; *Nep. m.*, *Nephila madagascariensis*; *Nep. s.*, *Nephila senegalensis*; *Lat. g.*, *Lactrodectus geometricus*; *Arg.t.*, *Argiope trifasciata*; *Arg. a.*, *Argiope aurantia*; *Gas. m.*, *Gasteracantha mammosa*; *Ara. b.*, *Araneus bicentenarius*; *Ara. d.*, *Araneus diadematus*; *Tet. k.*, *Tetragnatha kanaiensis*; *Tet. v.*, *Tetragnatha versicolor*. (Lewis 2006)

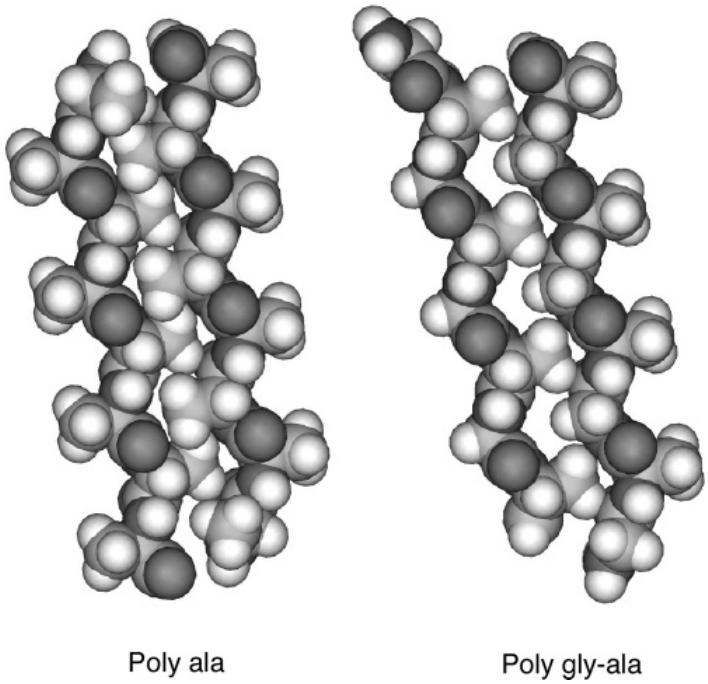

Fig. 1-5 Computer models of the poly-Ala and poly-(Gly-Ala) segment shown with two chains oriented in the vertical direction (Lewis, 2006)

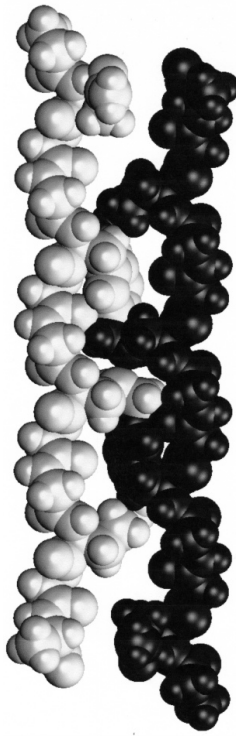

Fig. 1-6 Computer model of the GGX repeat region. The model is a space-filling energy-minimized antipallel two-strand GGS region. The starting configuration was a GlyII helix for both strands (Lewis 2006).

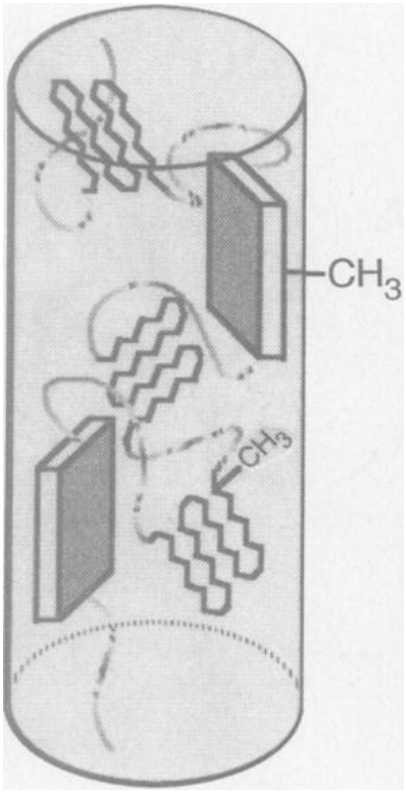

Fig. 1-7 Model for the molecular arrangement of the alanine residues in the dragline silk fiber. Highly oriented alanine-rich crystals of β-sheets (rectangles) and weakly oriented yet crystalline unaggregated sheets (canted sheet-like structures) are depicted in an amorphous glycine-rich matrix (curved line). The arrowindicates the fiber axis. (Simmons, Michal and Jelinski, 1996)

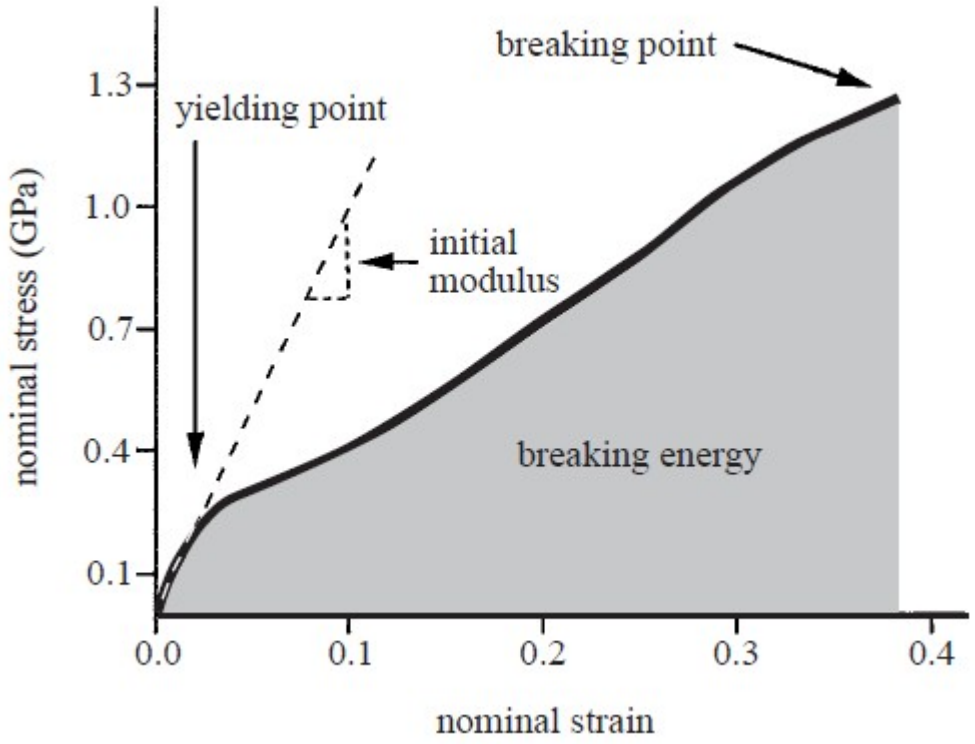

Fig.1-8 Typical stress-strain curve of a single major ampullate dragline thread from *Nephila edulis*. The curve starts to deviate significantly from the first linear part at the yielding point, thus showing yielding stress. The thread snaps at the breaking point allowing us to calculate the breaking stress and breaking strain. Further parameters calculated from the stress-strain curves were the initial modulus (the slope of the first linear part of the curve) and breaking energy (the area covered by the curve). (Gosline et al. 1999, Vollrath et al.2001a)

Chapter 2

Structural characteristics and properties of *Argiope amoena* dragline silk fiber obtained by different reeling speed

Chapter 2: Structural characteristics and properties of *Argiope amoena* dragline silk fiber obtained by different reeling speed

2. 1. Introduction

Spider dragline silk, the main structural web silk, is also used for the spider's lifeline, is widely studied mainly because of its excellent comprehensive mechanical properties, often considered superior to those of the tough synthetic fiber, Kevlar (X. Chen et al., 2006; Z. Shao et al., 1999; D. Porter et al. 2005). Wherever a spider goes, it leaves a silken trail, or dragline, behind. For a spider, the breaking stress of the material is a priority, and thus the silk must not break when fully loaded under normal conditions. Other material properties are also important, such as its initial resistance to stretching and the extension at which it finally breaks. Under different conditions, a spider might choose to crawl slowly or move quickly, for example when suspecting danger, escaping enemies or catching prey. The variations of moving speed lead to a change of spinning speed. Spinning speed is shown to be a significant factor in determining the physical properties of dragline silk. Two spider species, *Araneus diadematus* and *Nephila edulis*, were studied to analyze the mechanical properties of their dragline silks collected at three different reeling speeds: slow (4.0 mm s^{-1}), medium (20 mm s^{-1}) and fast (100 mm s^{-1}). The breaking strength increased with an increase in reeling speed, while the breaking strain decreased. These relations persisted when the extrusion speeds were extended even further to the range of 0.1 mm s^{-1} to 400 mm s^{-1}(F. Vollrath,B. Madsen and Z. Shao, 2001). The same variation

of mechanical properties of dragline silk from *Nephila pilipes* were revealed with reeling speed over a range of 1 to 100 mm s^{-1}(N. Du et al., 2006)

The mechanical properties of silk are actually determined by its hierarchical structural (T. Lefèvre et al., 2007). Spider silks are semicrystalline biopolymers that consist of repeated sequences of amino acids. Recently, research has revealed that dragline silk contain $(GA)_n/(A)_n$, GPGQQ and GGX peptide motifs which are repeated several times. These sequences make up the secondary structure of spider dragline silks divided into crystalline (β-crystalline) and non-crystalline (amorphous) domains (A. D. Parkhe1 et al., 1997; A. Bram et al., 1997; A. Simmons et al., 1994; J. Kümmerlen et al., 1996; A. H. Simmons et al., 1996). Successful silk assembly is based on extending, aligning and packaging of the individual silk proteins in the laminar flow inside the spinning duct. Hydrophobic residues (typically polyalanines of the repetitive coreregion) align upon multimerization initiated by the terminal domains and additionally by shear forces in the spinning duct. These polyalanine segments thereby expose an increasingly hydrophobic surface, which triggers the formation of β-sheet structures with numerous intra- and inter-chain hydrogen bonds (L. Römer et al., 2008; T. Scheibel, 2004). These β-sheet structures act as a reinforcement and contribute to the strength and stiffness of the silk. It has been found that the mechanical properties of the silk are affected by the level of crystallinity, the size and distribution of the crystallites, and the conformational and orientational organization at the molecular level (J. D. van Beek et al., 2002;M. E. Rousseau et al., 2004; J. M. Gosline et al. 1986). These silk structures are significantly influenced by the spinning process.

The East Asian species of orb-weaving spider, *Argiope amoena* is known in Japan as the “kogane-gumo”. *A. amoena* is a relatively large spider in Japan, with black and

yellow stripes on its torso. The body length of a female adult spider is usually 20-25 mm. It structures its web with a large zigzag pattern at the center called the stabilimentum. Recently, a short bundle consisting of 190,000 dragline filaments collected from *A. amoena* spiders was successfully used to support the body weight of an adult human male (S. Osaki, 2006). Strong violin strings that generate a soft and profound timbre were successfully prepared by twisting bundles of dragline filaments collected from *A. amoena* spiders (S. Osaki, 2012).

I examined the tensile strength of dragline filaments collected from *A. amoena* to determine whether they show a tendency to increase with reeling speed, as is the case for filaments gathered from *A. diadematus*, *N. edulis* and *N. pilipes*. In this paper we report the mechanical properties, the molecular structure, and the orientation of *A. amoena* dragline silk obtained by artificial forcible reeling at different speeds. The results indicate that the breaking stress and initial modulus of *A. amoena* dragline silk reach a maximum at reeling speeds of 20 mm s^{-1} and that *A. amoena* dragline silk reeled at 20 mm s^{-1} contains the most β-sheet polypeptides.

2.2. Materials and methods

2.2.1. Materials

Mature *A. amoena* spiders were caught in Kagoshima, Japan. The spiders were kept in the laboratory and bred in a box (100×90×30 cm) on a diet of silkworm moths.

2.2.2 Preparation of silk fiber

All dragline silk fibers were reeled directly from a healthy restrained spider that was fully awake. The spiders were made to crawl over a horizontal plane. When the spiders began to spin their dragline silk, they were held in a fixed position by hand.

The end of the dragline silk was taped to a roller and reeled at a controlled speed. The spider was fixed with a tape on a stage of stereoscopic microscope, facing upwards. A single silk strand was drawn under stereoscopic observation. The roller was positioned 15 cm above the spider's spinnerets. The drawing speeds used to study the mechanical properties of the silk were 2, 7, 11, 20, 60 and 100 mm s^{-1}, and those used to study the crystalline structure and molecular orientation of the silk were 4, 11, 20, 60 and 100 mm s^{-1}. Silk samples were collected at ambient room conditions of 20± 1°C and 35±5% RH from low to fast speeds. Minimum lengths of 2 m (for slow speeds) and a maximum of 20 m (for fast speeds) of silk fiber were collected. Only the last 50 cm of the silk fiber was sampled for each speed in tensile measurements. If a silk fiber was broken during sampling, this silk was excluded from measurements.

2.2.3. Tensile test of silk fibers

All measured samples were obtained from the same spider at different speeds to reduce variability. The original fibers were cut into shorter lengths (about 30 mm) to prepare samples for tests. These were mounted across rectangular holes cut in paper sheet supports to define the gauge length (20 mm) of mechanical test specimens. The fibers were fixed to the sheets using glue. All samples were stored in the test environment for 24 h to allow them to reach an equilibrium state.

The tensile properties of silk fiber samples were measured using a Tensilon Model UTM-II-20 (Orientec Corporation, Lachute, Canada). Tensile tests were carried out on 10 samples at each drawing speed. Before testing, the silk was brought to a zero tension position so that it neither sagged nor pulled the force transducer. All measurements were carried out at 25°Cand 65% RH at a gauge length of 20 mm and strain rate of 100%.A 5 N load cell was used. The silk was stretched until it broke.

Each value reported in the results in Section 3 is the average of 10 measurements.

One-way analysis of variance (ANOVA) in SPSS 17.0 was used to compare breaking stress, breaking strain, initial modulus and breaking energy of dragline silk fiber obtained at different speeds.

Cross-sectional images of the dragline silk fibers were recorded by a JEOL JSM-6010 LA scanning electron microscope (observation conditions: V=10 kV, I=0.06 nA). Dragline silk samples were sputter-coated with gold for 40 s before imaging. The images were used to confirm the presence of a single filament in each sample and to measure the sample diameter at 10 different positions along the gauge length. Computer image manipulation software was used to calculate the average cross-sectional areas of the spider dragline silk fibers.

2.2.4. Conformation of silk fibers

One thousand dragline silk filaments were aligned for Fourier transform infrared (FT-IR) spectroscopy performed using a Shimadzu FT-IR-8400S infrared spectrometer in ATR mode over the region of 4000-400 cm^{-1} at room temperature.

The determination of the secondary structure of proteins was done using a method that combined the second derivative, deconvolution, and band fitting. Quantitative information was obtained from the deconvolution of the amide I band (S. Ling et al., 2011; E. Bramanti et al., 1996).

The number and position of the components of the experimental spectrum were determined using the following criteria: 1) the minimum number of components; 2) second derivatives spectra. Before curve fitting, a linear baseline was subtracted. Four-point smoothing was used prior to obtaining the second derivative spectra. Band decomposition was performed using Gaussian band shapes. The peak positions were

fixed during the deconvolution process, and the bandwidth was automatically adjusted by Origin 7.5 software. The area under the different fitting peaks can be associated to the different types of the secondary structure.

2.2.5. Crystalline structure of silk fibers

One thousand spider dragline silk filaments were closely aligned and twined on a cardboard which had a hole of about 5 mm. Wide angle X-ray diffraction (XRD) profiles were obtained by a Rigaku Rotorflex RU-200B diffractometer using Ni-filtered Cu Kα radiation (wavelength of 0.1542 nm)generated at 40 kV and 150 mA.

2.3. Results and discussion

2.3.1 Sample geometry

After tensile testing, the geometry of each sample was studied by SEM. To allow for variations in the cross-sectional area and shape, micrographs were recorded at two different positions along the sample, in each case at two different orientations (0°-90°). The orientation was changed by rotating the sample about its long axis in the microscope. An example of a pair of micrographs recorded at 0° and 90° in Fig. 2-1.

Result are summarized in Table 2-1, the shape anisotropy is calculated as the ratio of D_0 (or D_{90}, whichever number is greater) to D_{90} (or D_0, whichever number is smaller); subscripts denote the sample orientation. Shape anisotropy is an indicator of the departure from a circular cross-section. Provided that the shape anisotropy is less than 1.2 (J. Pérez-Rigueiro, 2001), the cross-sections of the extruded silk fibers are closely approximated as circles with experimentally measured diameters. The

diameters and shape anisotropies of dragline silk fibers reeled at different speeds are summarized in Table 2-1. The shape anisotropy varies from 1.05 to 1.07. Therefore, the cross-section of the dragline fibers obtained by forced reeling can be reasonably regarded as circular.

2.3.2. Diameter of dragline fibers

Table 2-1 shows the relationship between the reeling speed and the diameter of *A. amoena* dragline fiber. The diameter increases with increasing reeling speed up to 11 mm s^{-1} and decreases with further increasing reeling speed from 11 to 100 mm s^{-1}. Samples from other *A. amoena* spiders also showed a similar trend, where the diameter had a maximum value when the reeling speeds ranged from 11 to 20 mm s^{-1}. This indicates that the diameter of *A. amoena* dragline silk does not have a linear relationship with the reeling speed. The majority of spider silk glands are a reservoir of soluble silk protein synthesized in specialized cells at the distal end of the gland and secreted into the lumen of the gland. The soluble silk is then pulled down a narrow duct, during which physical and chemical changes occur, producing the solid fiber. A muscular valve is present at the exit to the spinneret to control the flow rate of the fiber and can also be used to control the fiber diameter (R. V. Lewis, 2006). The results show that the forced reeling speeds have a stronger influence on diameter than the *A. amoena*'s own control abilities.

2.3.3. Tensile properties of dragline fibers

The breaking stress, breaking strain, initial modulus and breaking energy of *A. amoena* dragline fibers were obtained from stress-strain curves and are summarized in Fig. 2-2. The reeling speed significantly affected these four mechanical properties

(ANOVA, $p<0.01$). At reeling speeds of 20 mm s^{-1}, the breaking stress was found to be 1.41 GPa. This significantly varied for all other reeling speeds. In our study, the dragline fiber from ten different *A. amoena* spiders all showed similar regularity with maximum breaking stresses found at 11 and 20 mm s^{-1}. These results indicate significant differences in the breaking stress of dragline silk fibers from previously reported different species of spider (F. Vollrath et al., 2001; N. Du et al., 2006). *A. amoena* seem to have weaker endurance to reeling speed than *A. diadematus*, *N. edulis* and *N. pilipes*. This is not surprising as the spiders chosen have different biologies. The breaking strain decreased with increased reeling speeds, particularly with speeds at 4 mm s^{-1}. There was no significant difference in the breaking energy between the first four speeds, although it dropped significantly at higher speeds. The effect of reeling speed on breaking energy and breaking strain from *A. amoena* is similar to that observed for *N. edulis* (F. Vollrath et al., 2001).

Our measuring equipment was highly accurate, and our measuring conditions were fully controlled. The results from our experiment were highly consistent and thus reliable. The inter-individual variability of stress-strain properties was observed according to the nutritional state of the spiders and other factors. In each individual, reeling speed has shown a measurable effect.

2.3.4. Conformation of dragline fibers

The amide group of proteins and polypeptides present characteristic vibrational modes (amide modes), which are sensitive to the protein conformation. Amide I (1700-1600 cm^{-1} region) can be assigned primarily from the C=O stretching vibration, amide II (1600-1648 cm^{-1} region) is represented by the coupling of the N-H in-plane bending and C-N stretching modes, and amide III (1350-1190 cm^{-1} region) is

indicated by the C-N stretching coupled to the in-plane N-H bending mode. Vibrations of certain amino acid side chains have absorption bands within 1480-1350 and 1190-700 cm^{-1} region and may contribute slightly to the intensity of characteristic protein amide bands (E. Bramanti et al., 2005). In order to study the change of the fibroins conformation, dragline fibers obtained by different reeling speed were measured with FT-IR.

The amide I band of draglines collected at different reeling speeds was analyzed by applying the deconvolution procedure, where the percentage of each amide I component was obtained. Fig. 2-3 shows the comparison of FT-IR absorption spectra in the amide I region of all samples with reconstructed spectra. The assignment of the absorption peak in the amide I band is generally agreed upon: the peak from 1610 to 1640 cm^{-1} is attributed to a β-sheet conformation; the peak from 1640 to 1650 cm^{-1} is attributed to a random-coil conformation; the peak from 1652 to 1660 cm^{-1} is generally considered to be characteristic of a α-helix structure or other helical structures; the 3_1-helix has an amide I absorption peak in the range of 1658-1663 cm^{-1}; the peak from 1668 to 1691 cm^{-1} is attributed to a β-turn conformation. In addition, the simultaneous presence of the components at 1695 ± 4 cm^{-1} is typical of antiparallel (↑↓) β-sheets (E. Bramanti et al., 2005; J. M. Hadden et al. 1995).

The amide I band was deconvoluted using a Gaussian function as shown in Fig 2-3. The assignment of the negative peaks displayed in the second-derivative spectra corresponds to the frequencies of amide I components obtained after deconvolution (Table 2-2). This represents a fundamental step in order to correlate the percentage values of the recognized amide I components and the amounts of different secondary structures in the protein (Table 2-3). Quantitative analyses reveal that the secondary structure of the spidroin obtained at 20 mm s^{-1} contains 63.17% of β-sheets (including

antiparallel) more than others. This increase in the β-sheet content in the amide I band may play an important role in contributing to the fiber's high mechanical performance. However, the results also show that the amide I band of dragline silk reeled at 20 mm s^{-1} contain the fewest random structures, which suggests that some random structures are transformed into β-sheet structures during the reeling process. Using polarized Raman spectrometry, Pan *et al.* observed that *Araneus ventricosus* spider dragline silk drawn at 20 mm s^{-1} contained the most β-sheet polypeptides with high orientation structures. Our data regarding *A. amoena* dragline fibers resemble those obtained for *A. ventricosus* dragline fibers.

2.3.5. Crystalline structure of dragline fibers

The mechanical properties of silk should be determined at the molecular level by a number of structural factors, such as crystallinity, crystallite size and orientation. XRD is generally used to study the crystalline structure of the material. The natural dragline samples have broad XRD peaks at 2θ = 10-35° (A. D. Parkhe et al., 1997; A. H. Simmons et al., 1994, 1996). These sharp peaks in the XRD patterns show that the ordered phase of silk has an anti-parallel β-sheet structure. XRD patterns of dragline silk obtained by different reeling speed are shown in Fig 2-4. Dragline silk has a characteristic XRD peak at about 2θ = 20°. These vary slightly under different reeling speeds. Crystallinity, crystallite size and the orientation coefficient of the fibers obtained by different reeling speeds are shown in Table 2-4. A generalized structure of spider silk is considered to have crystalline regions in an amorphous matrix. When percent crystallinity is determined via XRD, the crystallinity is calculated by dividing the total area of crystalline peaks by the total area under the diffraction curve (crystalline plus amorphous peaks). According to Scherrer's formula, the crystallite

size is: $L = 0.9\lambda / FWHM(\cos\theta)$, where FWHM is the full width at half-maximum of the peak at the diffraction angle of θ and λ=1.5418 Å (Cu, Kα). Jade software was used on the XRD patterns to determine that the maximum crystallinity value (14.26%), and smallest crystallite size (3.16 nm) appeared at a reeling speed of 20 mm s^{-1}. The crystalline orientation of the fibers was determined quantitatively by Herman's orientation factor: $f = (3 <\cos^2\phi > -1)/2$, where ϕ is the angle between the *x*-crystallographic axis and the fiber axis. The parameter *f* is 0 when there is no preferred orientation in the fibers and 1 if all crystals are perfectly aligned with respect to each other (N. Du et al. 2006). As shown in Fig. 2-5, it appears that the orientation of the crystallites reaches an equilibrium value (orientation function f = 0.86) at a reeling speed of 20 mm s^{-1} and remains constant at higher reeling speeds, which is consistent with other observations.

A much higher stress is likely to be generated during rapid extension in the duct. The process of spinning the fiber has been described in detail by Vollrath et al. (2001). With increasing the reeling speed, the higher flow stress will affect the flow of liquid silk protein in the spider's gland and duct, bringing the spinning dope molecules into alignment and into a more extended conformation. This allows them to join together using hydrogen bonds like zip fasteners to give the anti-parallel beta conformation of the final thread, resulting in stiffer and stronger but less extensible fibers (Vollrath et al., 2001). However, for *A. amoena* spiders, when the dragline fiber is reeled at speeds over 20 mm s^{-1}, it becomes difficult to supply enough liquid silk protein with the appropriate composition in such a short time. Therefore, some molecular aggregation defects form during the liquid crystalline spinning process. The internal aggregation structure of the *A. amoena* dragline fibers is subsequently destroyed, the intermolecular bond of a spun silk may be fractured, and the β-sheet component and

crystallinity decreases, leading to a decrease in breaking stress. In addition, the crystallite size of *A. amoena* dragline fiber reaches a minimum value at 20 mm s^{-1}. Crystallite size has been theoretically calculated to affect silk tensile properties, with smaller crystallites increasing tensile strength more than larger crystallites (Y. Termonia, 1994). This can be attributed to smaller crystals resulting in a smaller number of defects in the crystallites. The orientation function also increases with reeling speed from 0.81 for 4 mm s^{-1} to 0.87 for 100 mm s^{-1}. When the silk is stretched at speeds over 20 mm s^{-1}, even though the orientation is nearly the same as produced at 20 mm s^{-1}, the decrease in crystallinity and increase of crystallite size may contribute to the dope of the breaking stress at high speeds. *A. amoena* and previously-reported spiders responded differently to the reeling speed treatments, suggesting differences in their basic silk properties.

Table 2-1 The diameter and shape anisotropy of dragline fibers reeled at different speeds from spider *A. amoena*

Reeling speed (mm s^{-1})	Mean fiber diameter (μm)	Shape Anisotropy
2	6.32 ± 0.26	1.05 ± 0.02
7	6.95 ± 0.29	1.07 ± 0.02
11	7.36 ± 0.21	1.05 ± 0.02
20	6.73 ± 0.28	1.06 ± 0.02
60	6.45 ± 0.18	1.05 ± 0.03
100	6.14 ± 0.16	1.05 ± 0.02

Table 2-2 Secondary structure analysis of silk proteins

	Wavenumber (cm^{-1})				
assignment	4 mm s^{-1}	11 mm s^{-1}	20 mm s^{-1}	60 mm s^{-1}	100 mm s^{-1}
β-sheet	1624.06	1624.06	1625.99	1624.06	1624.06
Random	1647.21	1647.21	1643.50	1651.07	1649.13
Helix	1663.50	1663.50	1660.71	1660.71	1660.71
Turns	1681.93	1681.93	1679.99	1685.79	1681.93
(↑↓)β-sheet	1695.43	1697.36	1693.5	1697.36	1697.36

Table 2-3 Proportions of the secondary structures in the silk proteins

Reeling speed	Secondary structure proportions (%)			
(mm s^{-1})	β-sheet	Random	Helix	Turns
4	53.51	24.02	17.50	5.96
11	55.54	22.02	12.80	9.63
20	63.17	5.02	29.33	2.47
60	53.72	21.45	19.63	6.19
100	51.86	25.36	13.59	9.19

Table 2-4 Crystallinity and crystallite size of dragline silk fiber dragline fibers reeled at different speeds fromspider *A. amoena*

Reeling speed (mm s^{-1})	Crystallinity (%)	Crystallinite size (nm)
4	11.03	4.11
11	11.58	3.54
20	14.26	3.16
60	11.25	4.03
100	10.57	4.72

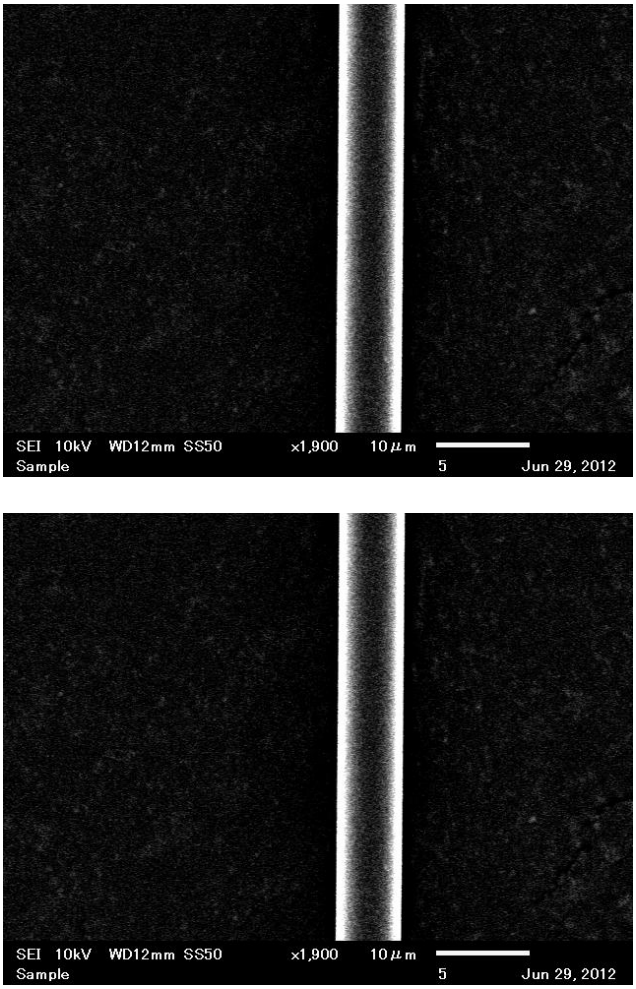

Fig. 2-1 Scanning electron microscopy images of dragline monofilament. The two orientations are related by a 90° rotation about the long axis of the sample.

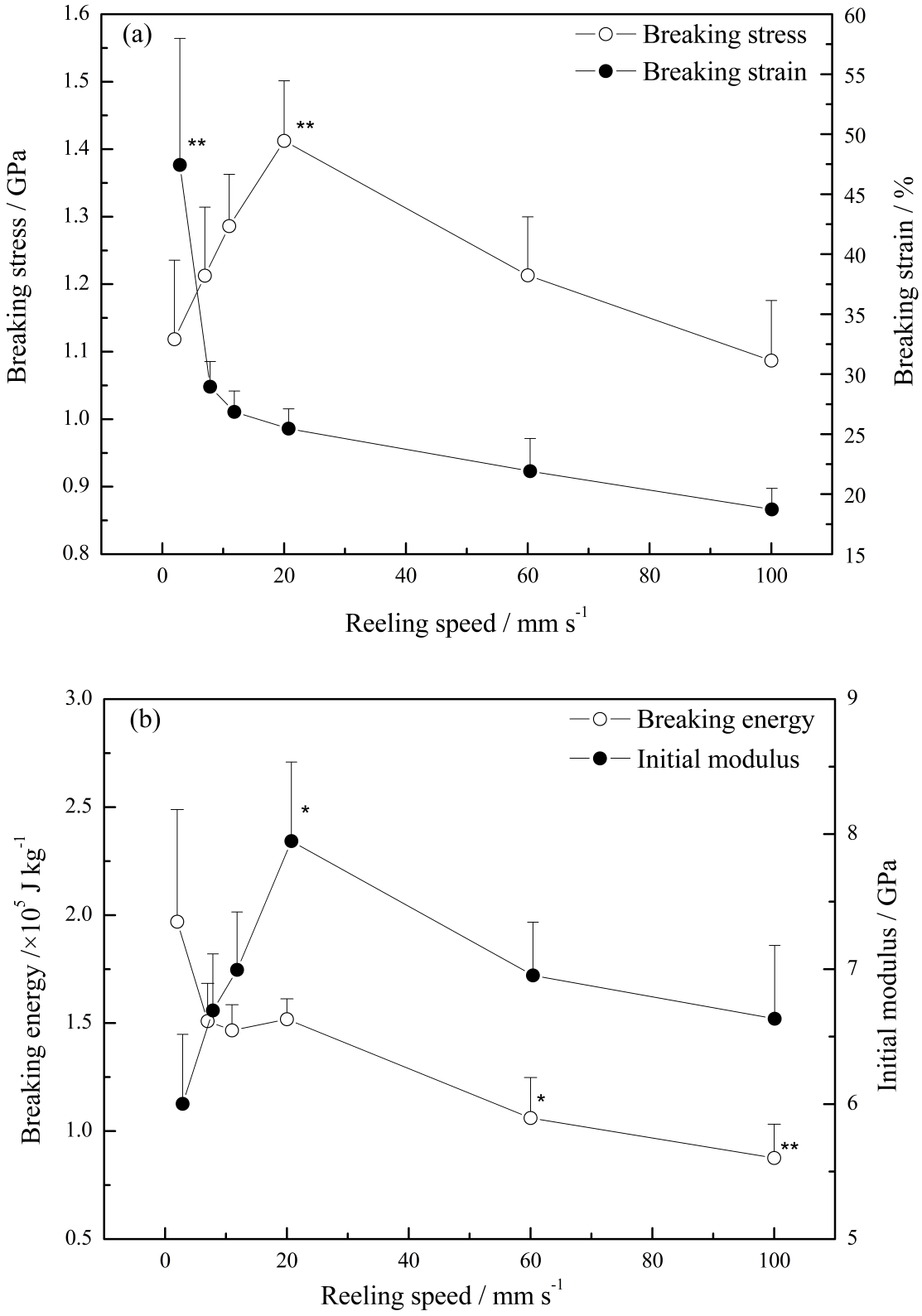

Fig. 2-2 Effects of reeling speed on (a) stress and strain at breaking, and (b) the initial modulus and breaking energy of *A. amoena* dragline fibers. Values are expressed as mean ± S.D. (n=10), * P<0.05 vs. other groups; ** p<0.01 vs. other groups.

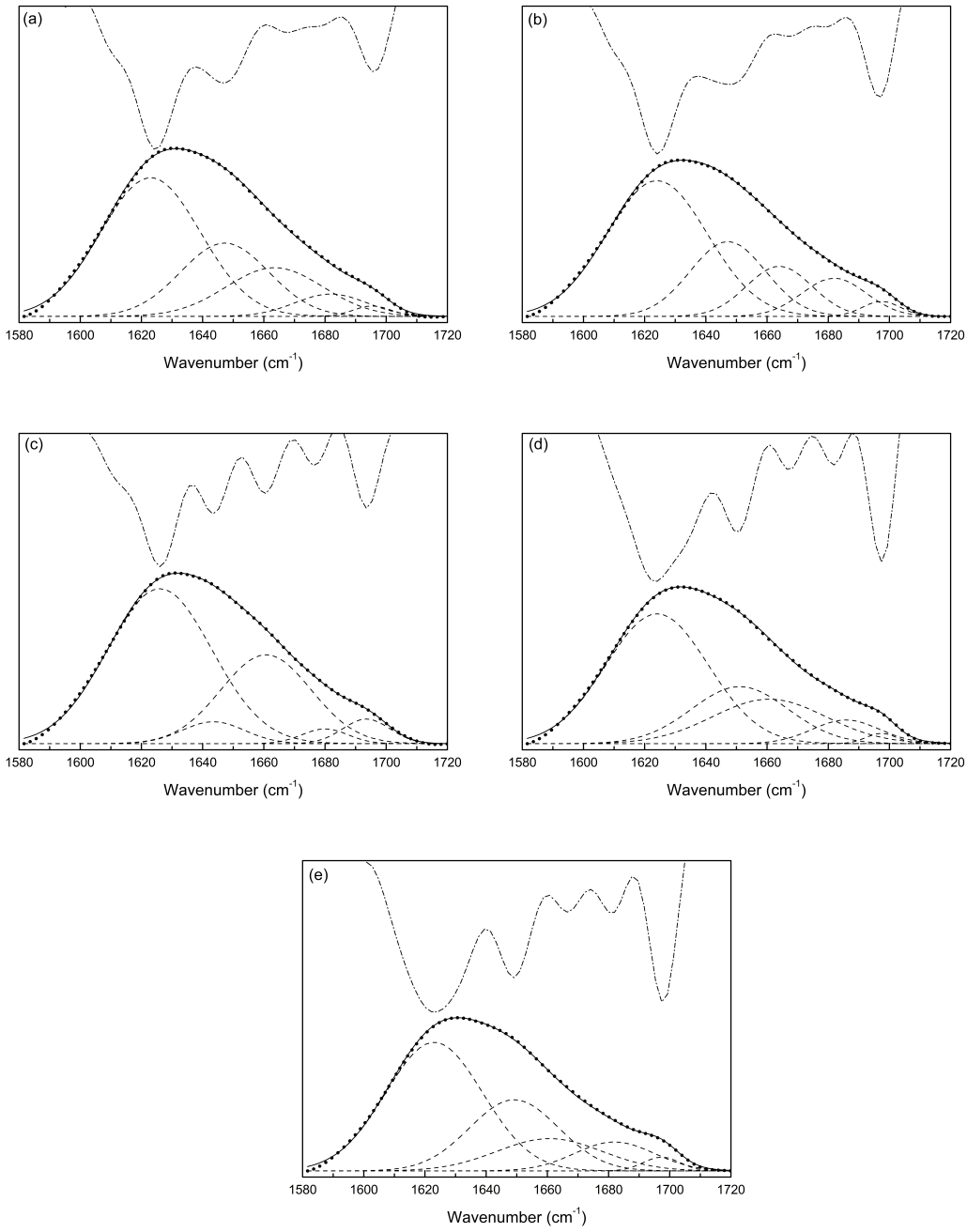

Fig. 2-3 Amide I region from *A. amoena* dragline fibers original FT-IR spectrogram (dotted line) with second derivative (dash dot line) above and component bands obtained through curve-fitting analysis below (solid line, fitting curve; dash line, deconvoluted peaks). Dragline fibers drawn at different reeling speeds: (a) 4 mm s^{-1}; (b) 11 mm s^{-1}; (c) 20 mm s^{-1}; (d) 60 mm s^{-1}; (e) 100 mm s^{-1}.

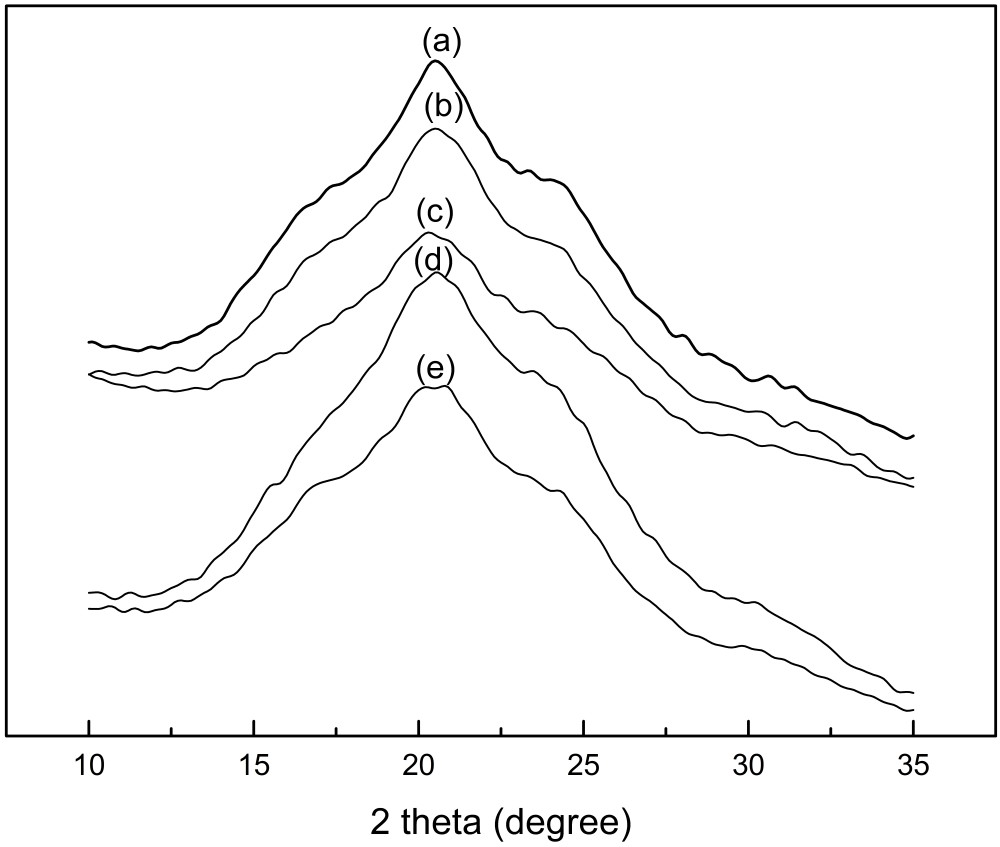

Fig. 2-4 XRD patterns of *A. amoena* dragline fibers drawn at different reeling speeds: (a) 4 mm s^{-1}; (b) 11 mm s^{-1}; (c) 20 mm s^{-1}; (d) 60 mm s^{-1}; (e) 100 mm s^{-1}.

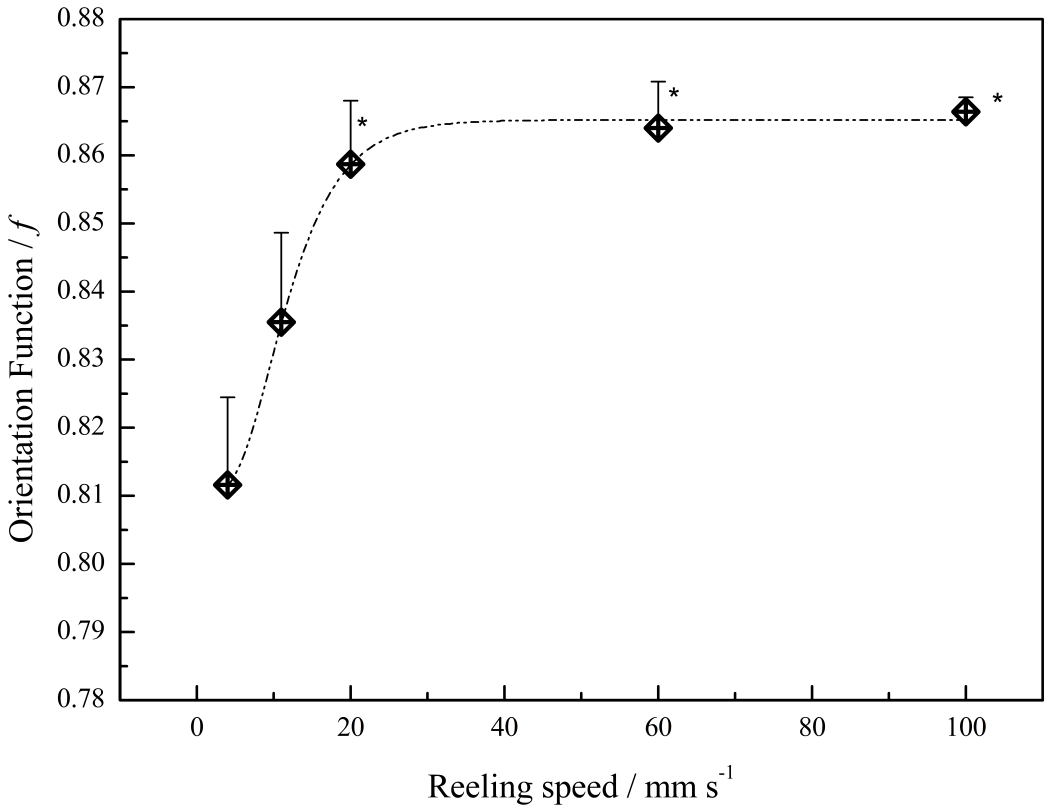

Fig. 2-5 Relationship between reeling speed and orientation function *f*.

Chapter 3

The variability of mechanical properties and molecular conformation among different spider dragline fibers

Chapter 3: The variability of mechanical properties and molecular conformation among different spider dragline fibers

3.1 Introduction

Spider silk is a protein fiber spun by spiders. Among all the spider silks, dragline silk is the most renowned for its high tensile strength, extensibility and toughness (Heim et al. 2009, Fu et al. 2009). In recent years, the mechanical properties of spider silks have aroused considerable interest. Research on the mechanical behavior of spider silk has shown that spider silk is an extremely variable biomaterial, variation in both the internal environment (e.g. pH and temperature) of the spider's silk gland (Dicko et al., 2004, Gaines et al., 2010, Eles and Michal, 2004) and external conditions (e.g. drawing speed and humidity) (Vollrath et al., 2001a, Vehoff et al., 2007) under which fibers are pulled from the spinnerets can influence silk properties. Even on the interspecific, intraspecific and intraindividual level, the mechanical properties displayed significant difference (Madsen et al. 1999). Spinning speed is also shown to be a significant factor for determining the mechanical properties: the spider fibers drawns at different speeds exhibit different tensile properties (Vollrath et al., 2001, Du et al., 2006).

Due to the availability of recombinant spider silk proteins, scientists will be able to

analyze the assembly of spider silk threads in a functional in vitro spinning process in the near future. This process has to ensure that the generated silk fiber resembles natural silk in its microstructure, chemical composition and mechanical properties.

The source of spider silk's remarkable properties has been attributed to the specific secondary and tertiary structures of proteins in the fiber (Hayashi et al., 1999). Dragline silk is secreted by the major ampullate gland, which gives rise to a hierarchically organized, semicrystalline material. The crystalline phase is made of short polyalanine segments that adopt a β-sheet conformation. Recent investigations have revealed that β-sheet crystals play a key role in the mechanical properties of silk (Bratzel and Buehler, 2011), improving strength and stiffness.

In this paper, I present and discuss the different mechanical properties of dragline silk fibers. I use tensile testing to characterize the mechanical properties of dragline fibers from four spider species: *Nephia clavata*, *Nephia pilipes*, *Argiope bruennichi* and *Argiope amoena*. Silk fibers were also forcibly reeled from four spiders under the different speeds. Additionally, I obtain Raman spectra and attempt to compare the molecular structure and orientation of these four spider dragline silk fibers.

3.2 Material and Methods

3.2.1 Spiders and silk fiber preparation

The spiders used were *Nephia pilipes* (from Ishikakijima, Japan), *Nephia clavata* (from Ueda, Japan), *Argiope bruennichi* (from Ueda, Japan) and *Argiope amoena* (from Kagoshima, Japan). These spiders all build orb webs. All of the spiders were

kept in the laboratory on a diet of silkworm moths. All dragline silk fibers were reeled directly from a restrained spider which is fully awake and healthy at reeling speeds of 2, 4, 7, 11, 20, 60 and 100 mm/s with a man-made device. All silk samples collected under the same conditions, and silk samples of each species spider were collected from same spider at ambient room condition of 20±1 °C and 35±5% RH. When varying the drawing speed, I waited at least 30 min, a minimum of 2 m (for slow speeds) and a maximum of 20 m (for fast speeds) of silk fiber was collected. Only the last 50 cm of a silk fiber sampled for each speed were used for any measurements. If a silk fiber broken during sampling, then this silk was exclude from measurements. The body weight of the spider is 4.5786 g, 3.1738 g, 1.1143 g and 3.4635 g, respectively. The silk fibers were collected and held on a black paper mandrel and studied within a week of collection at most.

The following measurements and experiments on the mechanical properties are presented in this paper: 1) a comparison of dragline fiber reeled at 20 mm/s from different species belonging to the two genera *Nephia* and *Argiope* and 2) a comparison of dragline fiber reeled from 2 to 100 mm/s from *N. pilipes*, *N. clavata* and *A. bruennichi*.

3.2.2 Tensile test of silk fibers

The tensile properties of the sample were measured with a Tensilon Model UTM-II-20 (Orientec Corporation). All measured silk samples for a given species were obtained from the same spider at different speeds to avoid variability. All measurements were carried out at 25°C and 65%RH at a gauge length of 20mm, a

pretension of 5 N and a tension rate speed of 10 mm min^{-1}. All samples were stored in the testing environment for 24 h to allow them to reach an equilibrium state. In addition, every sample was measured for 10 measurements.

The cross-sectional image of dragline silk fibers was recorded by a JEOL JSM-6010LA scanning electron microscope (observation conditions V=10 kV, I=0.06 nA). The dragline fibers were sputter-coated with gold for 40 s before measurement. The images were used to confirm the presence of a single filament in each sample and to measure the sample diameter at 10 different positions along the gauge length. Computer image manipulation software was used to calculate the average cross-sectional areas of the spider dragline silk fibers.

3.2.3 Conformation of silk fibers

Raman spectroscopy measurements were carried out on a HoloLab series 5000 Raman spectroscope (Kaiser optical systems, INC.). The 514 nm line of an Ar^+ laser was used. The laser beam was focused with a 50× objective (Olympus BX51) to a diameter of 2 μm, generating an intensity at the sample of 6 mW of power. The measurement time of a single spectrum was 110 sec, and accumulated 10 times. Every sample was measured 3 times, and an average Raman spectrum was calculated.

3.3 Results and discussion

3.3.1 Comparing the mechanical properties of dragline fibers from the four spider species

A dragline fiber was drawn from *N. clavata*, *N. pilipes*, *A. bruennichi* and *A.*

amoena spiders at reeling speed of 20 mm/s. The diameter and breaking force of the dragline and the spider's body weight are summarized in Table 3-1. The breaking force and diameter of the *N. clavata* and *A. amoena* fibers have a higher value than those of *N. pilipes* fibers, although *N. pilipes* is heavier in body weight than *N. clavata* and *A. amoena*. In general, larger spiders extruded proportionately thicker draglines with a stronger breaking force within the same spider species (Griffiths and Salanitri, 1980). Table 3-1 shows that this was not necessarily so when comparing the different spider species that were investigated. Dragline silk serves as a lifeline for spiders, so the relationship between the body weight of the spider and the breaking force is very important. Table 3-1 shows that there is a correlation between the body weight of a spider and the breaking force: the breaking force is one to three times the body weight. Griffith and Salanitri (1980) reported that the dragline could sustain two or three times the spider's weight, and Osaki (1999) reported that approximately six times the spider's weight corresponds to the breaking force. My result is quite similar to the result of Griffith and Salanitri, but is distinct from the result of Osaki.

The mechanical properties of four spider dragline fibers drawn at a reeling speed of 20 mm/s are shown in Fig. 3-1. The dragline fiber of *A. bruennichi* was relatively weak, while that of *N. clavata* was by far the strongest of the four spiders. The average maximum breaking stress of *N. clavata* dragline was 1.65 GPa, and the maximum initial modulus was 9.33 GPa. The following results were obtained when comparing the breaking stress within the same genus: *N. clavata>N. philips* and *A. amoena>A. bruennichi.* It is obvious that the mechanical properties of dragline among

different spider species are important variables.

3.3.2 Effect of the reeling speed on the mechanical properties

The breaking stress, breaking strain and initial modulus of dragline fibers of *N. clavata*, *N. pilipes* and *A. bruennichi* spiders were calculated. The effects of the reeling speed on the mechanical properties of three dragline fibers are shown in Fig. 3-2. As the reeling speed increased, the breaking strain of the dragline of the three spiders all decreased significantly, and the initial modulus slightly increased.

It has been reported that the breaking stress of draglines from *Araneus diadematus*, *Nephila edulis* and *N. pilipes* increased with increasing reeling speeds(Madsen et al. 1999). Du et al.(2006) reported that the breaking stress increased as the reeling speed increased and that the initial modulus increased until the reeling speed reached 20 mm/s, at which point it reached an equilibrium value. My data on *N. pilipes* dragline fibers were in agreement with Du's report. The breaking stress of *N. clavata* has a maximum value at a reeling speed of 11 mm/s. This result is very similar to the results for *A. amoena*, whose fiber has a maximum breaking stress value of 20 mm/s (chapter 1). With increasing the reeling speed, the breaking stress of *A. bruennichi* dragline fiber does not seem to vary.

3.3.3 The molecular structure of the four spider dragline fibers

Because Raman spectroscopy is now established as an important tool for studying the molecular structure of polymeric fibers (Vollrath, 2000, Sirichaisit et al., 2000), it was chosen to analyse the molecular structure of the dragline silk of *N. clavata*, *N.*

pilipes, *A. bruennichi* and *A. amoena*. For all of our measurements, I kept the direction of polarization of the laser radiation either fully parallel or fully perpendicular to the long axes of the silk fibers. Fig. 3-3 shows the Raman spectra of dragline silks of four spiders. It can be seen that a number of well-defined intense peaks can be obtained between 800 and 1800 cm^{-1}, with the Raman bands located at approximately 855, 905, 1094, 1230, 1399, 1450, 1615 and 1670 cm^{-1}. Different band shapes were observed for different spider genera. In particular, I note the scattering intensity of Raman bands at 1390 cm^{-1} in *Argiope* dragline fibers instead of the bands of 1399 cm^{-1} in *Nephia* dragline fibers when the direction of polarization of the laser beam is parallel to the fiber axis. This indicated that the isoquinoline compound is more prominent in the dragline fibers of *Argiope* (Lefèvre et al. 2011).

The amide I (1600-1700 cm^{-1}) and amide III (1200-1300 cm^{-1}) bands are particularly informative for protein fibers. The amide I and amide III bands of four spider fibers exhibit some differences between the parallel and perpendicular spectra, which is attributed to the anisotropy of the molecular arrangement. When the direction of polarization of the laser beam is perpendicular to the fiber axis, the amide I mode scattered most strongly. The Raman scattering intensity of the amide III mode is the largest when the polarized direction is parallel to the fiber axis. The amide I bands are located at approximately 1670 cm-1, which is characteristic of polyalanine segments with a β-sheet structure. The amide III bands exhibit some variation. When the polarization direction of the incident laser beam was perpendicular to the fiber axis, the peaks were located at approximately 1240 cm^{-1}, but when the polarization

direction of the incident laser beam was parallel to the fiber axis, the peaks were located at approximately 1228 cm^{-1}. The position of these bands is attributed to the β-sheet structure. This result is due to two modes with different symmetries of the antiparallel β-sheet unit cell (Lefèvre et al. 2011). In other sensitive peaks, the bands at approximately 1094 cm^{-1} and 1651 cm^{-1} are attributed to random coil and α-helix features, respectively.

A qualitative analysis of the Raman spectroscopy results to determine the β-sheet, α-helix and random coil content and the molecular orientation were performed(Shao et al., 1999b, Rousseau et al., 2004). The bands at 1670, 1651, and 1094 cm^{-1}originate from β-sheet, α-helix and random coil structures in silk proteins, while the band at 1452 cm^{-1} is insensitive to the protein conformation (Lefèvre et al. 2011). Consequently, the relative ratio of the intensity of 1670 cm-1 to 1451 cm^{-1} expresses the β-sheet content; the larger the values, the more extensive the β-sheet structure. The relative ratio of the intensity of 1670 cm^{-1} to 1651 cm^{-1} expresses the α-helix content; the larger the values, the less extensive the α-helix structure. The relative ratio of the intensity of 1670 cm^{-1} to 1094 cm^{-1} expresses the random coil content; As seen in Figure 3-3, the amide I band is stronger in the perpendicular spectrum whereas the amide III is stronger in the parallel spectrum. Since the amide I band is mostly associated with C=O stretching vibration, whereas the amide III mode has a major contribution from the C-N vibration, these results clearly show that the β-sheets are predominantly parallel to the fiber axis. Thus, the amide I and amide III bands vary in opposite directions as a function of polarization, so that their intensity ratio can be

used as a qualitative marker of the level of orientation (M. E. Rousseau. et al, 2004, Z.-J. Pan, and M. Liu, 2009) Semi-quantitatively parameters using the intensity ratio of $R=I_{\perp}/I_{\parallel}$ (amide I) and $I_{\parallel}/ I_{\perp}$ (amide III) can also be used, the larger the ratio value, the higher the degree of orientation. The relative intensity ratio within amide I or amide III can be used as a qualitative marker of the orientation level; the larger the ratio value, the higher the degree of orientation (Pan and Liu, 2009). The relative ratios of the Raman band values of four spiders' dragline fibers are summarized in Table 3-2. The result indicated that *N. clavata* spider dragline fiber had the largest I_{1670}/I_{1451}, suggesting that the *N. clavata* spider dragline fiber contained more β-sheet structures. The value of $I_{1670\perp}/I_{1670\parallel}$ express the degree of molecular orientation with the β-sheet structure. *N. clavata* spider dragline fiber also had the largest $I_{1670\perp}/I_{1670\parallel}$, suggesting that the orientation of the β-sheet molecular chains in dragline silk fibers of *N. clavata* is superior to that of the other three spider fibers. In addition, as indicated by the values of I_{1670}/I_{1451} and $I_{1670\perp}/I_{1670\parallel}$, within the same spider genus, β-sheet content and the degree of orientation in dragline fibers drawn at 20 mm/s, *N. clavata* is superior to *N. philips* and *A. amoena*is superior to *A. bruennichi.*

Table 3-1 The relationship between breaking force and body weight for four spiders for a reeling speed of 20 mm/s

	Body weight (N)	Diameter (μm)	Breaking force (N)
Nephia clavata	0.031	5.524±0.285	0.079±0.005
Nephia pilipes	0.045	5.385±0.142	0.054±0.003
Argiope bruennichi	0.011	2.922±0.093	0.015±0.002
Argiope amoena	0.034	6.734±0.279	0.100±0.007

Table 3-2 Relative ratio of the Raman band values of four spider dragline fibers for a reeling speed of 20 mm/s

Fiber	$I_{1670}/I_{1451}(\perp)$	$I_{1670}/I_{1451}(\parallel)$	$I_{1670}/I_{1651}(\perp)$	$I_{1670}/I_{1094}(\perp)$	$I_{1670\perp}/I_{1670\parallel}$
N. clavata	2.603	1.294	2.526	1.887	3.191
N. pilipes	2.235	1.113	2.142	2.616	2.887
A. bruennichi	1.764	0.894	1.974	2.595	1.780
A. amoena	2.018	0.985	1.994	2.367	1.940

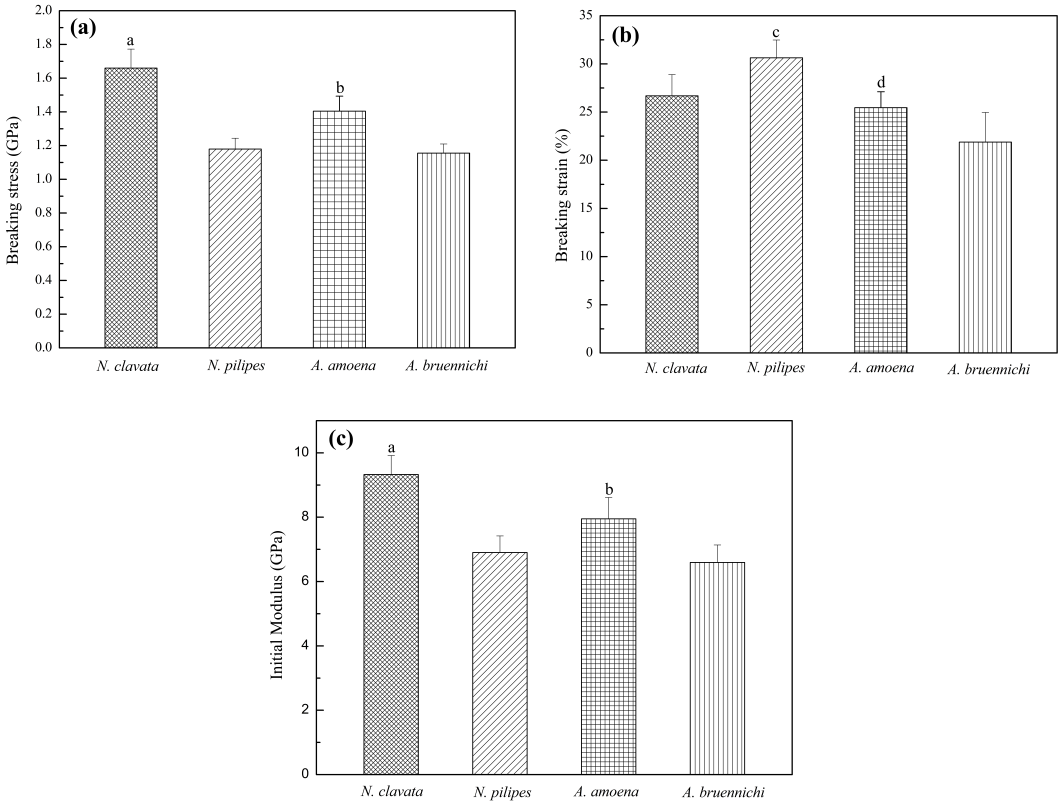

Fig. 3-1 Mechanical properties: (a) breaking stress, (b) breaking strain and (c) initial modulus of *Nephia clavata*, *Nephia pilipes*, *Argiope bruennichi* and *Argiope amoena* dragline fibers obtained at a reeling speed of 20 mm/s. Values are expressed as mean ± S.D. (n=10), a = P<0.01 vs. other groups; b = P<0.01 vs. *A. bruennichi*; c = P<0.05 vs. other groups; d= P<0.05 vs. *A. bruennichi*.

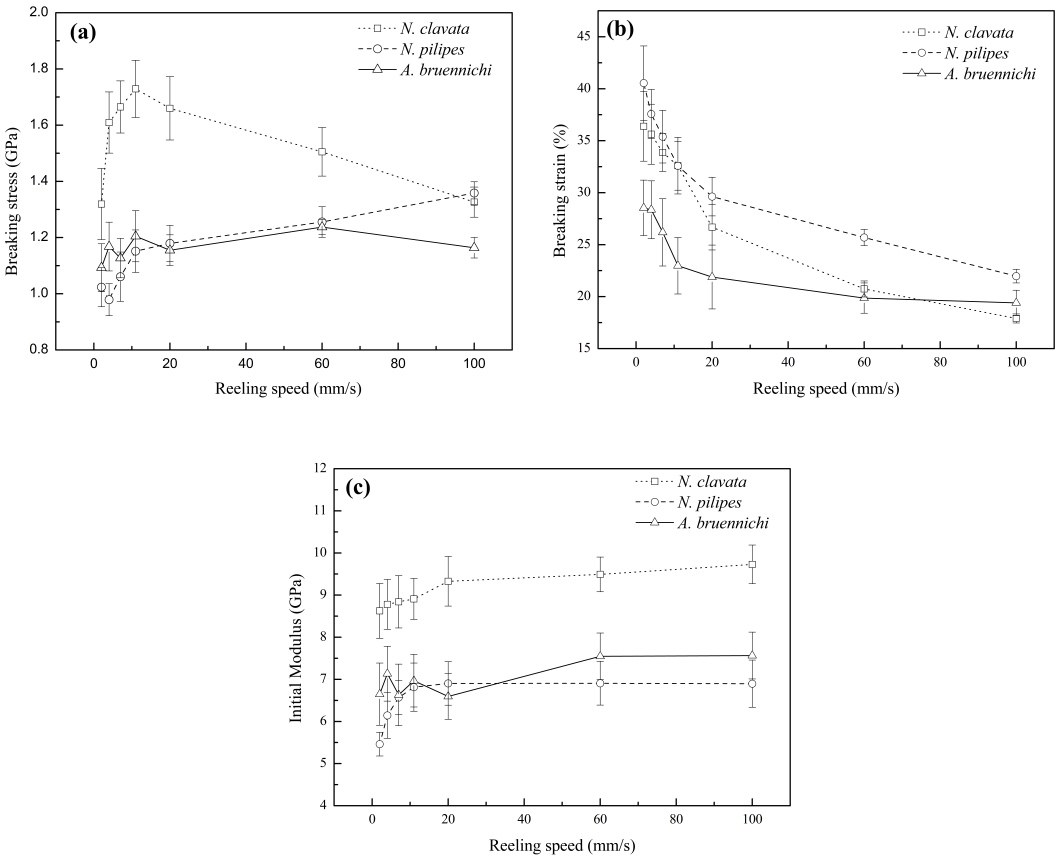

Fig. 3-2 The effects of reeling speed on the (a) breaking stress, (b) breaking strain and (c) initial modulus of *Nephia clavata*, *Nephia pilipes*, and *Argiope bruennichi* dragline fibers.

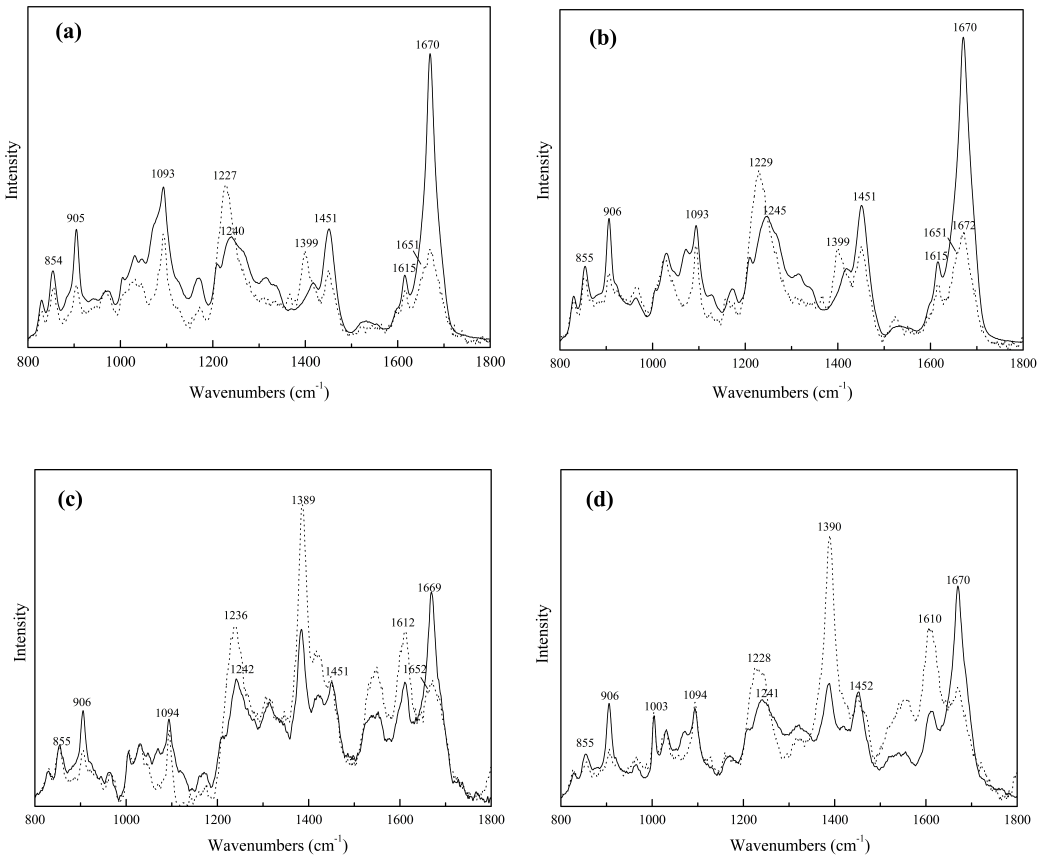

Fig.3-3 Raman spectra of dragline fibers of (a) *Nephia clavata*, (b) *Nephia pilipes*, (c) *Argiope bruennichi* and (d) *Argiope amoena* drawn at 20 mm/s. A single fiber was aligned either parallel (dashed line) or perpendicular (solid line) to the direction of the laser beam.

Chapter 4

Secondary structure analysis of spider dragline silk fiber obtained by different spinning methods using Raman spectroscopy

Chapter 4: Secondary structure analysis of spider dragline silk fiber obtained by different spinning methods using Raman spectroscopy

4.1 Introduction

Biomaterials, having evolved over millions of years, often exceed man-made materials in their properties. Silk is one of the most well-known biopolymers, possesses all of the most desirable textile fiber properties: superb fineness, strength, elasticity, dyeability, softness, flexibility, smoothness, luster, and elegance (Yuksek et al., 2000). Among silk fibers, spider silk has aroused considerable interest due to its combination of unique high tensile strength and extensibility (Vollrath and Knight, 2001b).

To adapt the sophisticated spinning machinery of spiders, several aspects have to be taken into account. Importantly, besides the protein composition of the spinning dope and the phase separation process in the spinning duct, several mechanical parameters play critical roles in silk assembly. In nature, spiders draw the thread with the hind legs (or by the force of gravity in case of roping) out of the spinning wart (Lewis, 2006, Riekel et al., 1999). This drawing process has been copied in the laboratory by forced silking of captive spiders. Interesting, large differences in resilience, ductility and thread diameters were reported depending on spinning speed and temperature.

For a full picture we need to use many different techniques. Various reports about silk monofilament structural information obtained with different techniques have been published. The techniques used include atomic force microscopy (AFM) (Du et al., 2006, Kane et al., 2010), scanning (Putthanarat et al., 2000) transmission electron microscopy (TEM) (Barghout et al., 1999, Augsten et al., 2000), Fourier transform infrared spectroscopy (FTIR) (Ling et al., 2011, Papadopoulosa et al., 2007), X-ray diffraction (XRD) (Du et al., 2006, Glišović and Salditt, 2007) and nuclear magnet resonance (NMR) (Creager et al., 2010, Yang and Asakura, 2005). These studies have yielded some useful information. However, Raman spectroscopy is particularly useful for analyzing the conformation of a material. The magnitude of the Raman bands depends on the chemical structure and morphology and the microstructure of the fiber. Meanwhile, Raman spectroscopy can provide both qualitative and quantitative information about protein conformations. Spider silk is composed almost entirely of protein (Hayashi et al., 1999). Using Raman spectroscopy to study the spider silk filament is the earliest research done to understand spider silk protein conformations. The ability to obtain well-defined Raman spectra from spider silk filaments has been demonstrated by Gillespie et al. (1994). Shao et al. (1999b, c) analyzed spider silk compositions in native and supercontracted states using Raman spectroscopy. The results showed that the differences in the mechanical properties were attributed to variations in the β-sheet content. Pézolet et al. calculated the order parameters P2 and P4 by Raman spectroscopy (Rousseau et al., 2004) and further tested the β-sheet orientation distribution function of silkworms *Bombyx mori* and *Samia cynthia ricini*

(Rousseau et al., 2006), dragline silk fibers of the spiders *Nephia clavipes* and *Nephila edulis* (Lefèvre et al., 2007), and flag silk fibers of the spiders *Araneus diadematus*, *Argiope aurantia* and *Nephila clavipes* (Lefèvre and Pézolet 2012). Pan et al. (2004) investigated the relationship between the microstructure and mechanical properties of spider dragline silk drawn by different methods using Raman spectroscopy.

In this study, Raman spectroscopy was used to investigate structural changes, particularly with respect to β-sheet conformation, in spider dragline silk fibers obtained by different spinning methods: crawl spinning, drop spinning and artificial reeling at 20 mm/s.

4.2 Material and method

4.2.1 Spiders and silk fiber preparation

The spiders used in this study were *Nephia clavata*, from the campus of Shinshu University, Japan. Dragline silk samples were collected by the following methods:

(1) Crawl spinning: placed the spider on a black table, allowed it to walk for at least 60-80 cm, while trailing silk behind it, silk was then collected.

(2) Drop spinning: placed the spider on a black table, collected the dragline silk when the spider vertically dropped off the edge.

(3) Artificial reeling: dragline silk was reeled directly from a restrained but fully awake spider at a drawing speed of 20 mm/s.

4.2.2 Methods

Raman spectroscopy measurements were performed with a HoloLab series 5000

Raman spectroscope (Kaiser optical systems, INC.). The 514 nm line of an Ar^+ laser was used. The laser beam was focused with a 50× objective (Olympus BX51) to a diameter of 2 μm, generating a intensity at the sample of 6 mW of power. The measurement time of a single spectrum was 110 sec, and 10 measurements were obtained. Every sample was measured 3 times, and an average Raman spectrum was calculated.

4.2.3 Data analysis (Lefèvre et al., 2007, Rousseau et al., 2006)

All spectral manipulations were performed using Origin 7.5. The spectra were first corrected for a small fluorescence background over the 500-1800 cm^{-1} spectral range using a polynomial baseline. The data were 5-points smoothed, and a linear baseline was subtracted in the amide I region (1750-1570 cm^{-1}).

Secondary structure composition was evaluated from the amide I band of the isotropic spectra. Because it consists of overlapping components due to the multiple secondary structures present in the sample, curve-fitting of the spectra have been necessary. The number and position of components of the experimental spectrum were determined using the following criteria in order of decreasing importance: (1) minimum number of components; (2) acknowledged secondary structures present in the considered system; (3) spectral criteria (shape of the experimental spectra, second derivatives and difference spectra.) and (4) generation of a reasonable fit (potentially requiring additional bands).

4.3 Result and discussion

4.3.1 Band assignments

The Raman spectrum of dragline silk fibers showed well-resolved peaks, including strong bands for the photosensitive aromatic amino acids tryptophan, tyrosine, and phenylalanine and for the amide I and amide III bands. The Raman spectrum in the region of 800-1800 cm^{-1} of dragline silk obtained by each spinning method is shown in Fig.4-1 and the Raman band assignments for silk listed in Table 4-1. The Raman band exhibited a minor difference between silk fibers obtained by different spinning methods.

4.3.2 Comparison among spider dragline silk obtained by different method

Fig.4-1 shows the Raman spectra of dragline silk obtained by spider spinning (crawl and drop spinning), compare to that of silk obtained by artificial reeling. In the drop spinning and artificial reeling spectra, both the amide I and amide III bands are centered at 1669 and near 1240 cm^{-1}, respectively, showing that the proteins in the silk exist in a β-sheet conformation. For crawl-spun fibers, the amide III band shift to 1250 cm^{-1} is attributable to random coil. These data indicate an obvious conformational change from the random coil in crawl-spun to β-sheets in the drop spinning and artificial-reeled fibers.

Other bands are aside from the amide bands are changed when dragline silk is obtained by different methods, particularly in the 1300-1400 cm^{-1} region and near 988 cm^{-1}. Two bands, one approximately 988 $cm^{-1}$and the other at 1354 cm^{-1} observed in

the spectra of spider spun silk, but these bands are absent in the spectrum of forcibly obtained silk. These bands mainly originate from the C-C skeletal stretch (988 cm^{-1}) and CH_2 deformation (1354 cm^{-1}).

The doublet bands located near 830 $cm^{-1}$and 854 cm^{-1} can be useful for monitoring the micro-environment around tyrosyl residues (Maiti et al., 2004). The tyrosyl doublet ratio (I854/I830) has been proposed as a means of determining whether tyrosine residue is solvent when exposed or buried in a hydrophobic environment. When the 850 cm^{-1} band is more intense than the 830 cm^{-1} band, the tyrosine residue is exposed. On the other hand, when I850 is less than I830, tyrosine residues are buried and tend to act as hydrogen donors. Fig.4-1 shows differences in the relative intensity of the tyrosine doublet at 830 and 854 cm^{-1}. The 853 cm^{-1} band for crawl-and drop-spun silks was less intense than the 830 cm^{-1}, indicating that the tyrosyl residue was buried. The 850 cm^{-1} band at for artificial reeled silk, however, was more intense than that at 830 cm^{-1}, indicating that, for this fiber, the tyrosine residues are exposed. This result suggests that hydrogen bonds involving tyrosyl residues are stronger in the spider spun silk than artificial reeled silk.

4.3.3 Quantitative analysis of fibroin conformation

Typical curve-fitting results for dragline silks created by different spinning methods are presented in Fig.4-2. An examination of these dragline silks revealed that the presence of five amide I components, located typically near 1641, 1655, 1669, 1684 and 1700 cm^{-1}, and two bands at 1596 and 1615 cm^{-1}, that are associated with tyrosine side-chain vibrations. Spectral decompositions are presented in Fig. 4-2 for dragline

silk fibers that were obtained by all three spinning methods. The position, full width at half maximum, and the individual components resulting from this spectral decomposition are give in Table 4-2. From these decomposed spectra, the proportions of α-helix, β-sheet, unordered and β-turn structures were calculated, and the obtained results are presented in Table 4-3. As observed in this table, silk obtained by different spinning methods exhibits different secondary structure concentrations. Compared among three spinning method, the artificial reeled silk fibers have maximum β-sheet content value and minimum α-helix content value is 42.94% and 8.48%, respectively. Crawl-spun silk exhibited a maximum α-helix content value and minimum β-sheet content value. These results mean that some of the α-helix, and perhaps some other structures, are transformed into β-sheet structure during the spinning process.

These results indicate that the secondary structure of spider silk could be modified by altering the spider's spinning environment. Indeed, the differences in secondary structure can be used in interpretation of biomechanical data. Higher *β*-sheet content can improve the silk strength and stiffness. These findings also suggest the tenacity of spider dragline silk fiber obtained by artificial reeling at 20 mm/s may be improved.

Table 4-1 Position and assignment of different bands of *N. clavipes* dragline silk obtained by three spinning methods

Crawl spinning	Drop spinning	Artificial reeling at 20 mm/s	Assignment
830	830	829	Tyr
854	854	854	Tyr
906	905	905	polyalanine
965	966	965	Ala
988	987		C-C stretch
1003	1003	1003	Phe
1030	1031	1030	Phe (in-plane stretching of benzene ring)
		1045	Pro
1067	1067	1075	Ser
1094	1094	1093	Cα-Cβstretching
1126	1126	1126	Leu
1168	1170	1170	Tyr
1209	1209	1209	Tyr
1252	1244	1240	Amide III (N-H bend +C-N stretching)
1334	1331		Ala
1354	1351		CH_2 deformation
1386	1386		C-C stretching of isoquinoline
1415	1417	1415	Gly
1450	1450	1450	CH_2, CH_3 bending modes
1524	1521	1528	C=C stretching of conjugated chain
1596	1596	1596	Tyr
1615	1615	1615	Tyr
1669	1669	1669	Amide I (C=O stretching)

Table 4-2 Results of amide I curve-fitting of *N. clavata* dragline silk obtained by three different spinning methods

		1	2	3	4	5	6	7
	Assignment			Unordered	α-helix	β-sheet	β-turn	β-turn
Crawl spinning	Position/cm^{-1}	1596	1615	1642	1656	1669	1684	1700
	FWHM/cm^{-1}	17	18	28	18	17	27	28
Drop spinning	Position/cm^{-1}	1596	1615	1641	1655	1669	1684	1700
	FWHM/cm^{-1}	19	17	29	16	18	29	31
Artificial reeling at 20 mm/s	Position/cm^{-1}	1596	1615	1641	1655	1669	1685	1700
	FWHM/cm^{-1}	17	20	24	16	18	23	25

Table 4-3 Percentages of secondary structure of *N. clavata* dragline silk obtained by three different spinning methods

	Unordered	α-helix	β-sheet	β-turn
Crawl spinning	15.51	11.79	35.97	36.71
Drop spinning	15.59	9.27	37.40	37.74
Artificial reeling at 20 mm/s	16.59	8.48	42.94	31.99

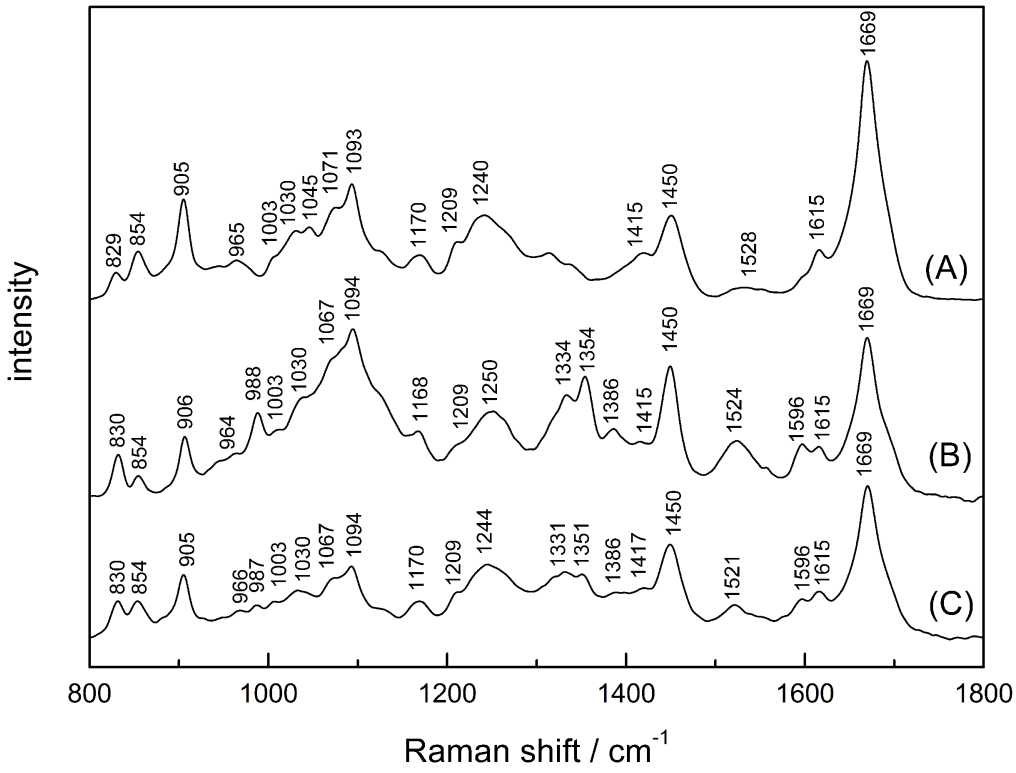

Fig.4-1 Raman spectra of *N. clavata* dragline silk fibers obtained by: (A) artificial reeling at 20 mm/s, (B) crawl spinning, and (C) drop spinning.

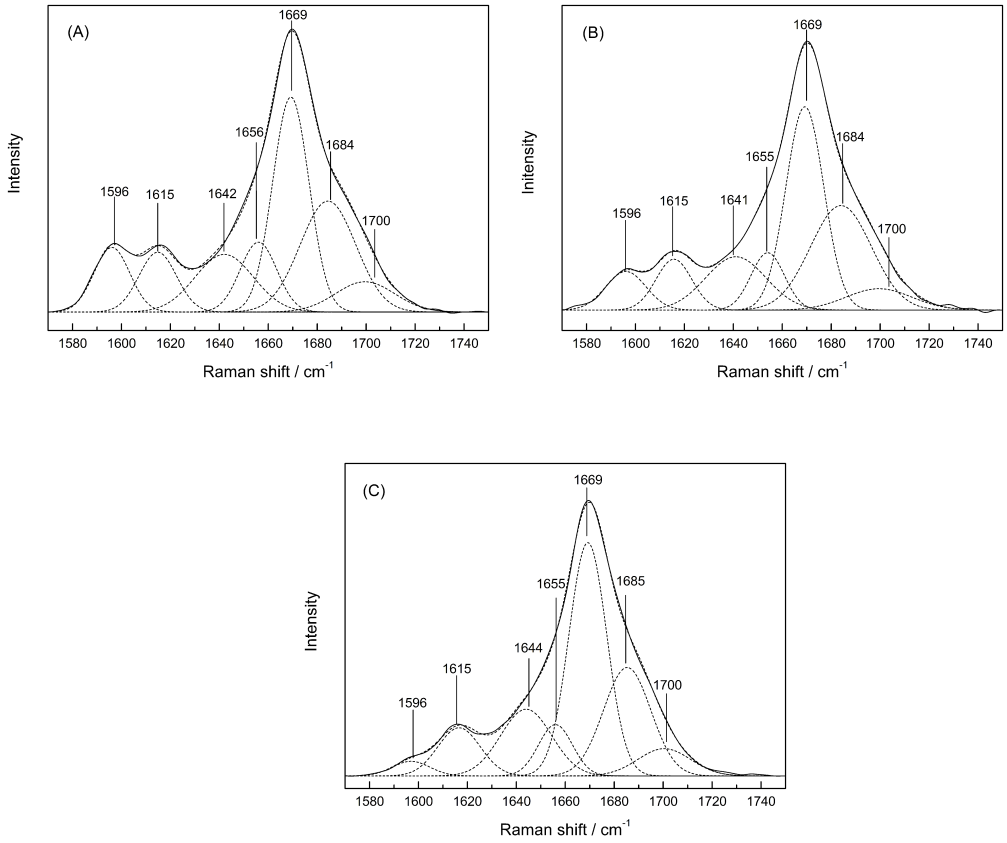

Fig.4-2 Band decomposition of the amide I region (1570-1750 cm^{-1}) of the polarized spectra for silk fibers obtained by: (A) crawl spinning, (B) drop spinning, and (C) artificial reeling at 20 mm/s.

Chapter 5

Summary

Chapter 5: Summary

Dragline silk, produced by spiders to form the outer rim and spokes of their webs, has long been admired for its remarkable mechanical properties such as high tensile strength and great extensibility. Meanwhile, the mechanical properties of spider dragline silk fibers are variable. The aim of this doctoral research is to analysis the variation by comparing the mechanical properties of silk produced by different spiders or in different conditions.

Chapter 2: Structural characteristics and properties of *Argiope amoena* dragline silk fiber obtained by different reeling speed

The tensile properties and structural characteristics of dragline fibers collected from *Argiope amoena* at different reeling speeds were determined. The strain at breaking decreased with increasing reeling speed. The breaking stress and initial modulus each showed a maximum value at a reeling speed of 20 mm s^{-1}; the average tension strength of the silk fibers was approximately 1.41 GPa. Crystallinity and orientation are important structural factors that determine the strength of spider dragline silk. The greatest amount of β-sheet structures occurs at 20 mm s^{-1}, which is most likely the natural reeling speed of spiders. The orientation of the crystallites in *A. amoena* dragline silk fibers increases up to a reeling speed of 20 mm s^{-1} and then reaches an equilibrium value. The strength of silk fibers can be enhanced by increasing both the β-sheet content and crystallinity and by decreasing crystallite size. Meanwhile, the mechanical properties of dragline silk are found to be significantly influenced by

reeling speed.

Chapter 3: The variability of mechanical properties and molecular conformation among different spider dragline fibers

This study has shown that the mechanical properties of spider dragline fiber are varied among the different species and affected by the reeling speed. In addition, we concluded from the obtained Raman spectra that the secondary structure content of the four spider dragline fibers is very different.

N. clavata dragline fiber shows a stronger breaking stress and initial modulus than the dragline fiber of *N. pilipes*, *A. bruennichi* and *A. amoena*. The mechanical properties of silk fiber should be determined at the molecular level by a number of structural factors, such as the crystallite structure and orientation. Our Raman spectra results show that the dragline fiber of *N. clavata* contains more β-sheet structures and a superior orientation than those of *N. pilipes*, *A. bruennichi* and *A. amoena*. These results demonstrate why the dragline fiber of *N. clavata* has stronger characteristics.

As the reeling speed increased from 2 to 100 mm/s, the breaking strains of three spider fibers decreased significantly, and their initial modulus increased. However, the breaking stresses of the different spider species exhibited different tendencies. The breaking stress of *N. clavata* dragline fiber has a maximum value at 11 mm/s. The breaking stress of *N. pilipes* dragline fiber increased as the reeling speed increased. In addition, the breaking stress of *A. bruennichi* dragline fiber maintains a relative stable value that is independent of the reeling speed.

A spider can actively control the diameter of the silk threads spun under different

environmental conditions. A larger spider also can spin a thinner silk fiber during the spinning process. In short, the mechanical properties of spider fibers are variable and can be affected by various conditions. Obtaining an excellent spider fiber requires many effect factors to be evaluated.

Chapter 4: Secondary structure analysis of spider dragline silk fiber obtained by different spinning methods using Raman spectroscopy

Raman spectroscopy is a useful tool for obtaining direct information on the secondary structural changes. When a high-performance polymer fiber is deformed, the stress applied is transformed directly into structural deformation, this deformation of in both crystalline and amorphous regions of the fiber cause a change in bond lengths, bond angles and internal rotation angles, which lead to a shift in the Raman frequency for a particular vibrational modes.

In this work, the conformation of the proteins in *N. clavata* dragline silk fibers obtained by three spinning methods was characterized. The obtained silk fibers exhibited a common structure characterized by the presence of β-sheet, unordered, β-turn and α-helix conformations. The presence of these secondary structures was determined through a curve-fitting procedure for the amide I band spectra, and the proportion of each within a fiber was found to vary with the spinning method. The quantity of β-sheet structures was greatly enhanced for silk fibers obtained by artificial reeling at 20 mm/s. This change may result in improved mechanical properties of dragline silk fiber, which has been helpful in designing an outstanding artificial spider silk.

In conclusion, the mechanical properties of spider dragline silk fibers are variable with accompany the changes of the silk protein secondary structure. Those variations not only appear in different species but also appear in different spinning condition. I expect that all of these studies will assist in producing high performance spider dragline silk fiber and will help to produce “artificial” spider silk.

References

References

Altman, G. H., Diaz, F., Jakuba, C., Calabro, T., Horan, R. L., Chen, J., Lu, H., Richmond, J.and Kaplan, D. L. (2003). Silk-based biomaterials, Biomaterials, 24, 401-416.

Augsten, K. Muhlig,P. and Herrmann, C. (2000). Glycoproteins and skin-core structure in *Nephila clavipes* spider silk observed by light and electron microscopy. Scanning, 22, 12-15.

Barghout, J.Y.J. Thiel, B.L. and Viney, C. (1999). Spider (*Araneus diadematus*) cocoon silk: a case of non-periodic latticecrystals with a twist? International Journal of Biological Macromolecules, 24, 211-217.

Boutry, C. and Blackledge, T. A. (2008). The common house spider alters the material and mechanical properties of orbweb silk in response to different prey. Journal of Experimental Zoology, 309A: 542-552.

Brookes, V. L., Young, R. J. and Vollrath, F. (2008). Deformation micromechanics of spider silk. J. Mater. Sci., 43, 3728–3732.

Brooks, A. E., Steinkraus, H. B., Nelson, S. R. and Lewis, R. V. (2005). An investigation of the divergence of major ampullate silk fibers from *Nephila clavipes* and *Argiope aurantia*. Biomacromolecules, 6, 3095–30999.

Bram, A., Branden, C. I., Craig, C., Snigireva, I. and Riekel, C. (1997). X-ray diffraction from single fibers of spider silk. J. Appl. Cryst., 30, 390-392.

Bratzel, G. and Buehler, M. J. (2011). Molecular mechanics of silk nanostructures under varied mechanical loading. Biopolymers, 97, 408-416.

Casem, M. L., Turner, D. and Houchin, K. (1999). Protein and amino acid composition of silksfrom the cob weaver, *Latrodectus hesperus* (black widow). Int J. Biol. Macromol., 24, 103-108.

Chen, X., Shao , Z. Z. and Vollrath , F. (2006).The spinning processes for spider silk. Soft Matter, 6. 448–451.

Chen, X., Knight, D. P. and Shao, Z. Z. (2009). Beta-turn formation during the conformation transition in silk fibroin. Soft Matter, 5(14), 2777-2781.

Craig, C.L. (1997). Evolution of arthropod silks. Annu. Rev. Entomol., 42, 231–267.

Creager, M. S., Jenkins, J. E., Thagard-Yeaman, L. A., Brooks, A. E., Jones, J. A., Lewis, R. V., Holland, G. P., Yarger, J. L. (2010). Solid-state NMR comparison of various spiders' dragline silk fiber. Biomacromolecules, 11, 2039-43

Cunniff, P. M., Fossey, S. A., Auerbach, M. A., Song, J. W., Kaplan, D. L., Adams, W. W., Eby, R. K., David, M. and Vezie, D.L. (1994a). Mechanical properties and thermal properties of dragline silk from the spider *Nephila clavipes*. Polym adv. technol., 5, 401-410.

Cunniff, P. M., Fossey, S. A., Auerbach, M. A. and Song, J. W (1994b). Mechanical properties of major ampullte gland silk fibers extracted from *Nephila clavipes* spider, In: silk polymers: Material Science and Biotechnology, ACS Symposium Series 544, Washington DC, 234-251

Dicko, C., Vollrath, F. and Kenney, J. M. (2004). Spider silk protein refolding is

controlled by changing pH. Biomacromolecules, 5, 704-710.

Dong, Z. Y., Lewis, R. V. and Middaugh, C. R. (1991). Molecular mechanism of spider silk elasticity. Arch Biochem Biophys, 284, 53-57.

Du, N., Liu, X. Y., Narayanan, J., Li, L., Lim, M. L. M. and Li, D. Q. (2006) Design of Superior Spider Silk: From Nanostructure to Mechanical Properties Biophysical Journal, 91, 4528-4535.

Eles, P. T. and Michal, C. A. (2004). A DECODER NMR study of backbone orientation in *Nephia clavipes* dragline silk under varying strain and draw rate. Biomacromolecules, 5, 661-665.

Foelix, R. F. (1996). Biology of spiders, 2nd Edition, Oxford University Press, Georg Thieme Verlag, New York, Chapter, 110.

Fu, C. J., Shao, Z. Z. and Vollrath, F. (2009). Animal silks: their structures, properties and artificial production. Chemical Communications, 6515.

Gaines, W. A., Sehorn, M. G. and Marrcotte W. R. (2010). Spidroin N-terminal domain promotes a pH-dependent association of silk proteins during self-assembly. Journal of Biological Chemistry, 285, 40745-40753.

Garrido, M. A., Elices, M., Viney, C. and Pérez-Rigueiro. J. (2002). Active control of spider silk strength: comparison of dragline spun on vertical and horizontal surfaces. Polymer, 43, 1537-1540.

Glišović, A. and T. Salditt. (2007). Temperature dependent structure of spider silk by X-ray diffraction. Appl. Phys. A., 87, 63–69.

Gillespie, D. B., Viney, C. and Yager, P. (1994). Raman-spectroscopic analysis of the

secondary structure of spider silk fiber.(Chapter 14) In Silk polymers: materials science andbiotechnology. Edited by Kaplan,D., Adams, W.W., Farmer,B.and Viney, C. American Chemical Society, Wastington. pp:155-167.

Gosline, J. M., DeMont, M. E. and Denny, M. W.(1986). The structure and properties of spider silk. Endeavour, 10, 37-43.

Gosline, J. M., Guererre, P. A., Ortlepp, C. S. and Savage, K. N. (1999). The mechanical design of spider: from fibroin sequence to mechanical function. J. Exp. Biol., 202, 3295-3303.

Griffiths, J. R. and Salanitri, V. R. (1980). The strength of spider silk. Journal of Materials Science. 15, 491-496.

Guerette, P. A., Ginzinger, D. G., Weber, B. H. F. and Gosline., J. M. (1996). Silk properties determined by gland specific expression of spider fibroin gene family. Science, 272, 112-115.

Hakimi, O., Knight, D., Vollrath, F. and Vadgama, P. (2007). Spider and mulberry silkworm silks as compatible biomaterials. Composites Part B: Engineering, 38, 324-337.

Harmer, A. M. T., Blackledge, T. A., Madin, J. S. and Herberstein, M. E. (2011). High-performance spider webs: integrating biomechanics, ecology and behavior. J. R. Soc. Interface, 8, 457-471.

Hayashi, C. Y., Shiply, N. H. and Lewis, R. V. (1999). Hypotheses that correlate the sequence, structural, and mechanical properties of spider silk proteins. Int. J. Biol. Macromol., 24, 271-275.

Hayashi, C.Y. and Lewis, R.V. (2001). Spider flagelliform silk: lessons in protein design, gene structure, and molecular evolution. Bioessays, 23, 750-756.

Heim, M., Keerl, D. and Scheibel, T. (2009). Spider Silk: From Soluble Protein to Extraordinary Fiber. Biomimetic Polymers, 48, 3584.

Herreo, A. M. (2008). Raman spectroscopy for monitoring protein structure in muscle food systems. Critical Reviews in Food Science and Nutrition, 48: 512-513.

Hinmam, M. B. and Lewis, R. V. (1992). Isolation of a clone encoding a second dragline silk fibroin. *Nephlia clavipes* dragline silk is a two-proten fiber. J. Biol. Chem., 267, 19320-19324.

Hinman, M. B., Jones, J. A. and Lewis R. V. (2000). Synthetic spider silk: a modular fiber. Trends Biotechnol., 18, 374-379.

Kane, D. M.,Naidoo, N. and Staib, G. R. (2010). Atomic force microscopy of orb-spider-web-silks to measure surfacenanostructuring and evaluate silk fibers per strand. JournalofApplied Physics, 108, 073509.

Khan, M. M. R., Morikawa, H., Gotoh, Y., Miura, M., Ming, Z, Sato, Y. and Iwasa. M. (2008). Structural characteristics and properties of *Bombyx mori* silk fiber obtained by different artificial forcibly silking speeds. Int. J. Biol. Macromol., 42, 264-270.

Knight, D. P., Knight, M. M. and Vollrath, F. (2000). Beta transition and stress-induced phase separation in the spinning of spider dragline silk. International Journal of Biological Macromolecules, 27, 205–210.

Lawrence, B. A., Vierra, C. A. and Moore, A. M. (2004). Molecular and mechanical

properties ofmajor ampullate silk of the black widow spider, *Latrodectus hesperus*. Biomacromolecules, 5, 689-95.

Lazaris, A., Aricidracono, S., Huang, Y. H. and Zhou, J. (2002). Spider Silk Fibers Spun from Soluble Recombinant Silk Produced in Mammalian Cells. Science, 295, 472–476.

Lefèvre, T., Rousseau, M. E. andPézolet, M. (2007). Protein secondary structure and orientation in silk as revealed by Raman spectromicroscopy. Biophysical Journal, 92, 2885-2895.

Lefèvre, T., Paquet-Mercier, F., Rioux- Dubé, J.-F. and Pézolet, M. (2011). Structure of silk by Raman Spectromicroscopy: from the spinning glands to the fibers. Biopolymers, 97, 322-336.

Lefèvre, T. and Pézolet, M. (2012). Unexpected β-sheets and molecular orientation in flagelliform spider silk of as revealed by Raman spectromicroscopy. Soft Matter, 1, 6350-6357.

Lewis, R. V.(2006). Spider silk: ancient ideas for new biomaterials. Chem. Rev., 106, 3762-3774.

Ling, S., Qi, Z., Knight, D. P., Shao, Z. Z. and Chen, X. (2011). Synchrotron FTIR microspectroscopy of single natural silk fibers. Biomacromolecules, 12, 3344-3349.

Lombardi, S. J. and Kaplan, D. L. (1990). The amino acid composition of major ampullate gland silk (dragline) of *Nephila clavipes* (Araneae, Tetragnathidae), J. Arachnol., 18, 297-306.

Lucas, F. (1964). Spiders and their silks. Discovery, 25, 2-26.

Motriuk-Smith, D., Smith, A., Hayashi, C.Y. and Lewis, R.V. (2005). Analysis of the conserved N-terminal domains in major ampullate spider silk proteins. Biomacromolecules, 6, 3152-3129.

Madsen, B., Shao, Z. Z. and Vollrath, F. (1999). Variability in the mechanical properties ofspider silks on three levels: interspecific, intraspecific and intraindividual. Int. J. Biol. Macromol., 24, 301-306.

Madsen, B. and Vollrath, F. (2000). Mechanics and morphology of silk drawn from anesthetized spiders. Naturwi ssenschaften, 87, 288-288.

Maiti, N. C., Apetri, M. M., Zagorski, M. G., Carey,P. R. and AndersonV. E. (2004). Raman spectroscopic characterization of secondary structure in natively unfolded proteins: alpha-synuclein. Journal of the American Chemical Society, 126 (8): 2399-408

Ortlepp, C. S. and Gosline, J. M. (2004). Consequences of forced silking. Biomacromolecules, 5, 727–731

Osaki, S. (1996). Spider silk as mechanical lifeline. Nature, 384, 419.

Osaki, S. (1999). Is the mechanical strength of spider's drag-lines reasonable as lifeline?. International Journal of Biological Macromolecules, 24, 283-287.

Osaki, S. (2006). Polymer Preprints, Japan 55, 1844.

Osaki, S. (2012). Spider silk violin strings with a unique packing structure generate a soft and profound timbre. Physical Review Letters, 108, 154301-154305.

Pan, Z. J., Li, C. P. and Xu. Q. (2004). Active Control on Molecular Conformations

and Tensile Properties of Spider Silk. Journal of Applied Polymer Science. 92, 901-905.

Pan, Z. J. and Liu, M. (2009). Effects of drawing speed and water on microstructure and mechanical properties of artificially spun spider dragline silk. Fibers and Polymers, 10, 285-289

Parkhe, A. D., Seeley, S. K., Gardner, K., Thompson, L. and Lewis, R. V. (1997). Structural studies of spider silk proteins in the fiber. J Mol Recog., 10, 1-6.

Papadopoulosa, P., Solter, J. and Kremer, F. (2007). Structure-property relationships in major ampullate spider silk as deduced from polarized FTIR spectroscopy. Eur. Phys. J. E., 24, 193-199.

Pauling, L. and Corey, R. B. (1953). Two pleated-sheet configurations of polypeptide chains involving both cis and trans amide groups. Proc. Nat. Acad. Sci. USA, 39, 247-252.

Pérez-Rigueiro, J., Elices, M., LLorca, J. and Viney, C. (2001a). Tensile Properties of *Argiope Trifasciata* Drag Line Silk Obtained from the Spider's Web. Journal of Applied Polymer Science, 82, 2245-2251.

Pérez-Rigueiro, J., Elices, M., LLorca, J. and Viney, C. (2001b). Tensile properties of silkworm silk obtained by forced silking. Journal of Applied Polymer Science, 82, 1928-1935.

Peakall, D. B. (1969). Synthesis of silk, mechanism and location. Am. Zoologist, 9, 71-79.

Porter, D., Vollrath F. and Shao, Z. (2005). Predicting the mechanical properties of

spider silk as a model nanostructured polymer, Eur. Phys. J. E., 16, 199–206.

Putthanarat, S., Stribeck, N., Fossey, S. A., Eby, R. K. and Adams, W. W. (2000). Investigation of the nanofibrils of silk fibers. Polymer, 41, 7735.

Reddy, R. M. and Prasad, G. V. (2011). Silk-the prospective and compatible bio-material for advanced functional applications. Trends Applied Sci. Res., 6, 89-95.

Riekel, C., Müller, M. and Vollrath F. (1999). In-situ X-ray diffraction studies during forced silking spider silk. Macromolecules, 32: 4464-4466

Rousseau, M. E., Lefèvre, T., Beaulieu, L., Asakura, T. and Pézolet, M. (2004). Study of protein conformation and orientation in silkworm and spider silk fibers using Raman microspectroscopy. Biomacromolecules, 5, 2247-2257.

Rousseau, M. E., Beaulieu, L., Lefèvre, T., Paradis, J., Asakura, T. and Pézolet, M. (2006). Characterization by Raman microspectroscopy of the strain-induced conformational transition in fibroin fibers from the silkworm *Samia cynthia ricini*. Biomacromolecules, 7, 2512-2521.

Römer, L. and Scheibel, T. (2008). The elaborate structure of spider silk Structure and function of a natural high performance fiber, Landes Bioscience, 2, 154.

Rössle, M., Panine, P., Urban, V. S. and Riekel, C. (2004). Structural evolution of regenerated silk fibroin under shear: Combined wide- and small-angle x-ray scattering experiments using synchrotron radiation. Biopolymers, 74, 316-327.

Scheibel, T. (2004). Spider silks: recombinant synthesis, assembly, spinning, and engineering of synthetic proteins. Microbial Cell Factories, 3:14.

Shao, Z. Z. and Vollrath, F. (1999a). The effect of solvents on the contraction and mechanical properties of spider silk. Polymer, 40, 1799-1806.

Shao, Z. Z., Vollrath, F., Sirichaisitb, J. and Young, R. J. (1999b). Analysis of spider silk in native and supercontracted states using Raman spectroscopy Polymer, 40, 2493-2500.

Shao, Z. Z. Young, R. J. and Vollrath, F. (1999c). The effect of solvents on spider silk studied by mechanical testing and single-fiber Raman spectroscopy. International Journal of Biological Macromolecules, 24, 295-300.

Shao, Z. Z. and Vollrath, F. (2002) Surprising strength of silkworm silk. Nature, 418,741

Simmons, A. H., Ray, E. and Jelinski, L. W. (1994). Solid-state C-13 NMR of *Nephila Clavipes* dragline silk establishes structure and identity of crystalline regions. Macromolecules, 27, 5235-5237.

Simmons, A. H., Michal, C. A. and Jelinski, L. W. (1996). Molecular orientation and two component nature of the crystalline fraction of spider dragline silk. Science, 271, 84-87.

Sirichaisit, J., Young, R. J. and Vollrath, F.(2000). Molecular deformation in spider dragline silk subjected to stress. Polymers, 41, 1223-1227.

Sirichaisit, J., Brookes, V. L. Young, R. J. and Vollath, F. (2003). Analysis of structure/property relationships in silkworm (*Bombyx mori*) and spider dragline (*Nephila edulis*) silks using Raman spectroscopy. Biomacromolecules, 4, 387-394.

Sponner, A., Schlott, B., Vollrath, F., Unger, E., Grosse, F. and Weisshart K. (2005) Characterization of the protein components of *Nephila clavipes* dragline silk. Biochemistry, 44, 4727-4736.

Swanson, B. O., Blackledge, T. A., Beltran, J. and Hayashi, C. Y. (2006). Variation in the material properties of spider dragline silk across species. Applied physics, 82, 213-218.

Termonia, Y. (1994). Molecular modeling of spider silk elasticity. Macromolecules, 27, 7378-7381.

Tsukada, M., Obo, M., Katoh, H., Freddi, G. and Zanetti, B. (1996). Structure of dye ability of *Bombyx mori* silk fibers with different filament sizes. J. Appl. Polym. Sci., 60, 1619-1627

Vehoff, T., Glišović, A., Schollmeyer, H., Zippelius, A. and Salditt T. (2007). Mechanical properties of spider dragline silk: humidity, hysteresis and relaxation. Biophysical Journal. 93, 4425-4432.

Vollrath, F.(1992). Spider webs and silks. Sci. Am., 266, 70.

Vollrath, F., Holtet, T., Thogersen, H. and Frische, S. (1996). Structural organization of spider silk. Proc. R. Soc. Lond. B 263, 147–51.

Vollrath, F. (2000). Strength and structure of spiders' silks, Review in Molecular biotechnology, 74, 67-83.

Vollrath, F., Madsen, B. and Shao, Z. Z. (2001a). The effect of spinning conditions on the mechanics of a spider's dragline silk. Proc. R. Soc. Lond Ser B-Biological Sciences, 268, 2339-2346.

Vollrath, F. and Knight, D. P. (2001b). Liquid crystalline spinning of spider silk. Nature, 410, 541–548

Winker, S. and Kaplan, D. L. (2000). Molecular biology of spider silk. Rev. Mol. Biophys. J., 78,2690-2701.

Work, R. W. and Young C. T. (1987). The amino acid compositions of major and minor ampullate silks of certain orb-web-building spiders (Araneae, Araneidae), J. Arachnol., 15, 65-80.

Xu, M. and Lewis, R. V. (1990). Structure of a protein super fiber: spider dragline silk. Proc. Natl. Acad. Sci. USA, 87, 7120-7124.

Yang, M. and Asakura, T. (2005). Design, expression and solid-state NMR characterization of silk-like materials constructed from sequences of spider silk, *Samia cynthia ricini* and *Bombyx mori* silk fibroins. J Biochem., 137, 721-729.

Yuksek, M., Kocak, D. Beyit, A. and Merdan, (2012). N. Effect of degumming performed with different type natural soaps and through ultrasonic method on the properties of silk fiber. Advances in Environmental Biology, 6(2), 801-808.

Zhang, Y., Yang, H. Shao, H. and Hu, X. (2010). *Antheraea pernyi*silk fiber: a potential resource for artificially biospinning spider dragline silk, Journal of Biomedicine and Biotechnology, 2010: 683962.

Acknowledgement

I would like to extend my best respects and regards to all the people involved in my thesis for their invaluable suggestion and help. Without their efforts, I would not complete my doctoral thesis favourably.

First of all, I would like to express my sincere appreciation to my supervisor Prof. Masao Nakagaki, Division of Applied Biology, Faculty of Textile Science and Technology, Shinshu University. He kindly provided me this opportunity to study in his laboratory, and gave me many good suggestions on experiments. His kindness and strictness will benefit all my life.

I would also like to thank Associate Prof. Yasuo Gotoh, Dr. Toshifumi Ikaga, Mr. Shouhei Koyama and Ms. Keiko Kakegawa. They gave me many helps, suggests during experiment.

I would also like to express my thanks to Prof. Masuhiro Tsukada, Prof. Mikihiko Miura, Prof. Toshio Shida and Prof. Hiroshi Moriwaki for their strict reviews and valuable advices over my doctoral thesis.

This work was supported by a Grant-in-Aid for Global COE Program by the Ministry of Education, Culture, Sports, Science, and Technology, Japan. I am indebted to Japanese government for awarding me a scholarship during this study.

A sincere gratitude should be expressed to the leaders and colleagues in Sericultural

Research Institute, Anhui Academy of Agricultural Sciences, China.

I wish to express my special and sincere thanks to Dr. Tianfu Zhao, Dr. Yujun Wang and Mr. Leng Han for their help and warmth toward me throughout my study. They supported me from the spirits and helped me to lead my life in Japan smoothly and happily.

Last but not least, the deepest appreciation and sincere gratitude are extended to my parents, my wife, my son, and all other members in my family for their love, devotion, understanding, and encouragement throughout my entire study in Japan.